Gaussian Random fields and monogenic images

Hermine Biermé, Philippe Carré, Céline Lacaux, Claire Launay

GAUSSIAN RANDOM FIELDS AND MONOGENIC IMAGES

HERMINE BIERMÉ, PHILIPPE CARRÉ, CÉLINE LACAUX, AND CLAIRE LAUNAY

Abstract. In this paper, we focus on lighthouse anisotropic fractional Brownian fields (AFBFs), whose self-similarity depends solely on the so-called Hurst parameter, while anisotropy is revealed through the opening angle of an oriented spectral cone. This fractional field generalizes fractional Brownian motion and models rough natural phenomena. Consequently, estimating the model parameters is a crucial issue for modeling and analyzing real data. This work introduces the representation of AFBFs using the monogenic transform. Combined with a multiscale analysis, the monogenic signal is built from the Riesz transform to extract local orientation and structural information from an image at different scales. We then exploit the monogenic signal to define new estimators of AFBF parameters in the particular case of lighthouse fields. We prove that the estimators of anisotropy and self-similarity index (called the Hurst index) are strongly consistent. We demonstrate that these estimators verify asymptotic normality with known variance. We also introduce an estimator of the texture orientation. We propose a numerical scheme for calculating the monogenic representation and strategies for computing the estimators. Numerical results illustrate the performance of these estimators. Regarding Hurst index estimation, estimators based on the monogenic representation of random fields appear to be more robust than those using only the Riesz transform. We show that both estimation methods outperform standard estimation procedures in the isotropic case and provide excellent results for all degrees of anisotropy.

Keywords: Gaussian field, Self-similarity, Anisotropy, Fractional Brownian field, Estimation, Hurst parameter, Monogenic signal, Riesz transform.

2010 Mathematics Subject Classification. Primary: 62M40,60G15, 62M30. Secondary: 60G22, 60-04, 62F12.

1. Introduction

Self-similarity characterizes an object that maintains the same properties at different scales. The self-similarity property especially allows to model some rough natural phenomena (see e.g [1, 33, 43, 49] for some applications in medicine, internet traffic, geophysics, hydrogeology or finance) and then a fractal analysis may provide help for classification of rough data (see e.g. [34] for a nice review in medical imaging). Moreover, it is particularly adapted to the analysis of micro-textures, which do not present any geometrical structure or pattern, and are usually modeled by a Gaussian random field. In medical imaging e.g., modeling a texture obtained by mammograms by a self-similar random field and studying its self-similarity order allow to distinguish between dense or fatty tissue. The most famous self-similar Gaussian field is the Fractional Brownian field (fBf) B_H with Hurst parameter $H \in (0,1)$, see [36, 31]. This fractional field generalizes the fractional Brownian motion and has been introduced to model rough natural phenomena. It is the only isotropic Gaussian centered random field H-self-similar with stationary increments. Moreover, its Hurst parameter H controls its smoothness: the smaller H is, the rougher the fractional Brownian texture.

The anisotropy of the data is also a very important characteristic to take into consideration in many applications, e.g. in medicine [10] or in geology [8, 17]. Then, the isotropy property of the fBf severely restricts its use in modelling. Several authors have then introduced anisotropic generalizations of the fBf, see for example [3, 16, 29, 32, 13]. Especially, in this paper, we are interested in anisotropic fractional Brownian fields (AFBFs) introduced in [16] and were used to model and analyse mammograms and bone radiography (see [9] for a survey). AFBFs still have stationary increments and are defined by a generalization of the fBf's harmonizable representation allowing the spectral density to vary with the direction. A self-similar AFBF is then characterized by a Hurst index H that controls its smoothness and an anisotropic function called the topothesy following [21]. Such fields, also called anisotropic scale-free models in [22], can be simulated using the turning-band method as proposed in [14] and implemented in the PyAFBF library [42]. In this paper, we more specifically focus on the class of random fields called elementary field in [14], renamed here lighthouse fields, in reference to Yves Meyer's lighthouse measures that are non negative Radon measure whose Fourier transform is supported by a double circular cone. For such a field the topothesy function is the indicator of a double cone, and then is characterized by an orientation and the cone opening angle. Such class of AFBFs includes fractional Brownian fields when the double cone covers the plane.

This work has been supported by the RT CNRS 2179, the RT CNRS 2169 and the project ANR-19-CE40-005 MISTIC. .

In practice, estimating the model parameters is a very important issue to model and analyse real data. In the literature, several estimators of the self-similarity index H have been proposed. We refer to [6, 20] and references therein for some reviews concerning long range dependent random processes and fractional Brownian motion. Especially two kinds of methods are quite popular in the literature. The first one relies on generalized quadratic variations, see e.g. [27] for self-similar Gaussian processes with stationary increments, [7, 19] for some Gaussian processes, [18] for stationary Gaussian fields or [15] for some anisotropic fractional Brownian fields with a spectral density. The second one is based on wavelets coefficients, see e.g. [23, 5] for the fractional Brownian motion. The Hurst parameter, estimated using a wavelet-based method, has been established by Abry et al. (see [48, 2]). As claimed by Abry et al., compared to other estimators the wavelet-based estimator performs well both statistically and computationally. Moreover, the wavelet-based method can also eliminate certain trends due to the property of its vanishing moments [2]. Several robust estimators have been proposed based on the standard wavelet-based estimator. For example, Soltani et al. [44] proposed an enhanced wavelet-based estimator by averaging two wavelet coefficients separated by half the length and taking the logarithm first or Feng et. al. [25] proposed a robust estimator of the Hurst parameter via general trimean estimators (a weighted average of the distribution's median and two quantiles symmetric about the median) of non-decimated wavelet coefficients.

Moreover, for a lighthouse field, it is also essential to characterize its degree of anisotropy. The degree of anisotropy can be analyzed using the coherence index associated with the calculation of the structure tensor [40]. However, particularly to naturally introduce a multiscale approach and complementary information, the monogenic approach is well-suited as it allows for the calculation of the coherence index and the direction of the field at different scales [37, 40]. Indeed, the monogenic signal, introduced in [24] is defined through the Riesz transform, an analog in dimension of the Hilbert transform which behaves like the gradient operator.

In this paper, we propose to use the monogenic signal [24] to analyse the class of lighthouse random fields. Studying this monogenic signal and using an analysis based on monogenic wavelets [45], we derive a first estimator of their self-similarity parameter H. Then, following [37, 40], inferring only the Riesz tensor, a part of the monogenic tensor, we propose a second estimator of the self-similarity parameter and also an estimator of the coherence index. For each proposed estimator, we establish consistency and asymptotic normality.

The paper is organized as follows. Section 2 introduces anisotropic self-similar Gaussian random fields having a spectral density and the subclass of vertically oriented lighthouses random fields. Next Section 3 focuses on the monogenic signal of a random field. Then Section 4 explains how the numerical experiments are performed, using a multiscale decomposition and illustrates the results obtained in Section 3. Then Section 5 studies the estimation of the Hurst parameter H of such a lighthouse random field using the monogenic signal. Section 6 is devoted to the inference of the coherence index and the Hurst index based on the Riesz structure tensor. Concerning the estimation of the Hurst index, this section also provides a comparison with the estimation using the monogenic signal and some other methods. Section 7 considers the case of a general lighthouse random field which orientation can be non vertical and introduces an estimator of its orientation as well as numerical results. All the proofs are postponed to the Appendix.

2. Anisotropic self-similar Gaussian random fields

One of the most studied examples of self-similar Gaussian random fields with stationary increments is the fractional Brownian field B_H with Hurst parameter $H \in (0,1)$. This random field is isotropic and the closer the Hurst parameter is to 0, the rougher the texture created. On the contrary, the closer H is to 1, the smoother the texture appears. To model scale invariant textures whose properties change according to the observed direction, we can consider some anisotropic self-similar Gaussian random fields introduced in [16]. Let us recall their definition.

Let W be an isotropic complex Gaussian measure on $\mathbb{R}^2$ with Lebesgue intensity (see e.g. [43] for details on such random measures). Then, for a complex-valued function $g : \mathbb{R}^2 \to \mathbb{C}$, the stochastic integral

$$W(g) := \int_{\mathbb{R}^2} g(\xi)\, W(d\xi)$$

is well-defined if and only if $g \in L^2_{\mathbb{C}}\left(\mathbb{R}^2\right)$, see [43]. Furthermore, for $g \in L^2_{\mathbb{C}}\left(\mathbb{R}^2\right)$, $W(g)$ is a Gaussian complex-valued random variable whose characteristic function is given by

$$\forall z \in \mathbb{C},\ \mathbb{E}\left(\exp\left(i\Re\left(\overline{z}W(g)\right)\right)\right) = \exp\left(-\frac{1}{2}\|W(g)\|_2^2\,|z|^2\right)$$

where

$$\|W(g)\|_2^2 = \int_{\mathbb{R}^2} |g(\xi)|^2 d\xi.$$

Therefore, we identify $W(g)$ with the random vector $(\Re(W(g)), \Im(W(g))$, a real-valued centered Gaussian vector whose covariance matrix is $\|W(g)\|_2^2\, I_2$. Moreover, this defines an isometry between complex-valued square integrable functions and complex Gaussian random variables with covariance structure given by, for all $g, g' \in L^2_{\mathbb{C}}(\mathbb{R}^2)$,

$$\mathbb{E}\left(\Re(W(g))\Re(W(g'))\right) = \mathbb{E}\left(\Im(W(g))\Im(W(g'))\right) = \Re(\langle g, g'\rangle) \tag{1}$$

$$\text{and } \mathbb{E}\left(\Im(W(g))\Re(W(g'))\right) = -\mathbb{E}\left(\Re(W(g))\Im(W(g'))\right) = \Im(\langle g, g'\rangle),$$

with

$$\langle g, g'\rangle = \int_{\mathbb{R}^2} g(\xi)\overline{g'(\xi)}d\xi = \frac{1}{2}\mathbb{E}\left(W(g)\overline{W(g')}\right).$$

Let now $f : \mathbb{R}^2 \to \mathbb{R}$ be a spectral density, that is an even non-negative function such that $f \in L^1\left(\mathbb{R}^2, \min(1, |\xi|^2)d\xi\right)$. Then the real-valued Gaussian random field X whose harmonizable representation is given by

$$X(x) := \Re\left(\int_{\mathbb{R}^2} [e^{-ix\cdot\xi} - 1]\sqrt{f(\xi)}\, W(d\xi)\right), \quad x \in \mathbb{R}^2 \tag{2}$$

is well-defined and has stationary increments. Moreover, if its spectral density f is an homogeneous function, i.e. if for $\xi \in \mathbb{R}^2\backslash\{0\}$

$$f(\xi) = t\left(\frac{\xi}{|\xi|}\right)|\xi|^{-2H-2}, \tag{3}$$

with $H \in (0, 1)$ and $t \in L^1(S^1)$ an even non-negative function defined on the unit sphere $S^1 \subset \mathbb{R}^2$, then the random field X is self-similar of order H, i.e. for every $\lambda > 0$

$$\{X(\lambda x); x \in \mathbb{R}^2\} \overset{(fdd)}{=} \lambda^H \{X(x); x \in \mathbb{R}^2\}$$

where $\overset{(fdd)}{=}$ means equality of finite dimensional distributions.

In the following, we will focus on the subclass of lighthouse fields, also called elementary fields in [14]. In this case, up to a rotation (see Section 7), the function t (respectively the spectral density f) is parameterized by $\delta \in (0, \pi/2]$ (respectively by (H, δ)) and then denoted by t_δ (respectively $f_{H,\delta}$).

Definition 2.1. *Let $H \in (0, 1)$, $\delta \in (0, \pi/2]$ and $t_\delta : S^1 \to [0, \infty)$ be the even function such that*

$$\forall \alpha \in (-\pi/2, \pi/2],\ t_\delta(\Theta(\alpha)) = \mathbf{1}_{|\alpha|\leq\delta}, \tag{4}$$

where

$$\Theta(\alpha) = (\cos(\alpha), \sin(\alpha)) \in S^1.$$

Moreover, let us consider the spectral density $f_{H,\delta}$ defined by

$$f_{H,\delta}(\xi) = t_\delta\left(\frac{\xi}{|\xi|}\right)|\xi|^{-2H-2},\ \textit{a.e. } \xi \in \mathbb{R}^2. \tag{5}$$

Then the random field X associated to $f_{H,\delta}$ by (2) is called lighthouse Gaussian random field with parameters (H, δ).

When $\delta = \pi/2$, the lighthouse field is the isotropic fractional Brownian field. Let us also mention that lighthouse fields can be simulated by the turning-band method (see [14]). Figure 1 shows four examples for $H = 0.5$ and multiple δ values. The closer δ gets to 0, the more horizontally oriented the spectral density is and the more vertically oriented the texture appears.

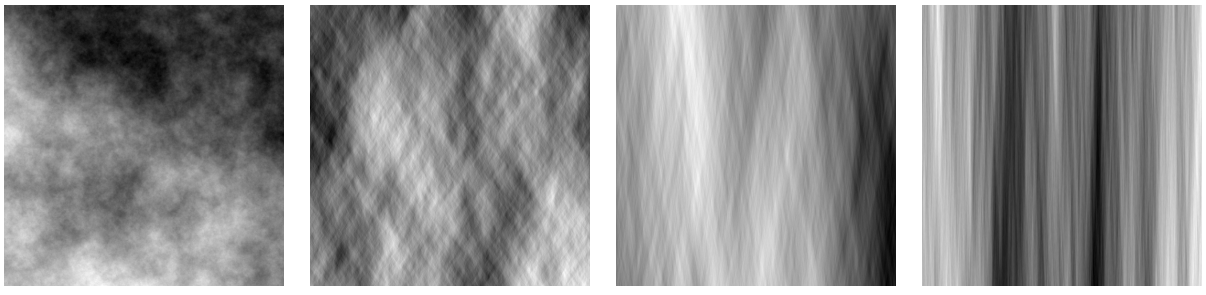

a) $\delta = \pi/2$ b) $\delta = \pi/4$ c) $\delta = \pi/12$ c) $\delta = \pi/64$

FIGURE 1. Realizations of lighthouse random fields for several values of δ and $H = 0.5$.

Finally, in this paper, we interpret the random field X defined by (2), with $f \in L^1(\mathbb{R}^2, \min(1, |\xi|^2)d\xi)$, in terms of a tempered distribution. For any function $u \in L^2(\mathbb{R}^2)$, let us first denote by $\widehat{u}$ its Fourier transform, with

$$\forall \xi \in \mathbb{R}^2,\ \widehat{u}(\xi) = \int_{\mathbb{R}^2} e^{-ix\cdot\xi}\, u(x)dx.$$

Then let us recall that the Schwartz space $\mathcal{S}(\mathbb{R}^2) \subset L^2(\mathbb{R}^2)$ consists of functions $u : \mathbb{R}^2 \to \mathbb{R}$ in $\mathcal{C}^\infty(\mathbb{R}^2)$ such that

$$\forall m \in \mathbb{N} \text{ and } j = (j_1, j_2) \in \mathbb{N}^2,\ \|u\|_{m,j} = \sup_{x\in\mathbb{R}^2} (1 + |x|)^m \left|D^j u(x)\right| < \infty.$$

We will mainly consider the subspace $\mathcal{S}_0(\mathbb{R}^2)$ consisting of functions $u \in \mathcal{S}(\mathbb{R}^2)$ such that

$$\widehat{u}(0) = \int_{\mathbb{R}^2} u(x)dx = 0$$

and sometimes $\mathcal{S}_1(\mathbb{R}^2) \subset \mathcal{S}_0(\mathbb{R}^2)$ with also $D^j\widehat{u}(0) = 0$ or equivalently

$$\int_{\mathbb{R}^2} x_1^{j_1} x_2^{j_2} u(x)dx = 0,$$

for $|j| = j_1 + j_2 = 1$.

For $u \in \mathcal{S}_0(\mathbb{R}^2)$, one has

$$\begin{aligned}\int_{\mathbb{R}^2}\left(\int_{\mathbb{R}^2}|e^{-ix\cdot\xi}-1|^2u(x)^2f(\xi)d\xi\right)^{1/2}dx &\leq 2\left(\int_{\mathbb{R}^2}\max(1,|x|)\,|u(x)|\,dx\right)\\ &\quad\times\left(\int_{\mathbb{R}^2}\min\left(1,|\xi|^2\right)f(\xi)d\xi\right)^{1/2}\\ &< +\infty\end{aligned}$$

since $f \in L^1\left(\mathbb{R}^2, \min\left(1,|\xi|^2\right)d\xi\right)$. Then, applying a generalization of the Fubini's stochastic theorem (see Theorem 2.1 of [39]), gives us that a.s.

$$\begin{aligned}\int_{\mathbb{R}^2}X(x)u(x)dx &= \Re\left(\int_{\mathbb{R}^2}\left(\int_{\mathbb{R}^2}[e^{-ix\cdot\xi}-1]\sqrt{f(\xi)}u(x)dx\right)W(d\xi)\right)\\ &= \Re\left(\int_{\mathbb{R}^2}\widehat{u}(\xi)\sqrt{f(\xi)}\,W(d\xi)\right),\end{aligned}$$

since $\widehat{u}(0) = 0$ and with $\widehat{u}\sqrt{f} \in L^2_{\mathbb{C}}\left(\mathbb{R}^2\right)$. Hence we set

$$\langle X, u\rangle = \Re\left(\int_{\mathbb{R}^2}\widehat{u}(\xi)\sqrt{f(\xi)}\,W(d\xi)\right). \tag{6}$$

The random field $(\langle X,u\rangle)_{u\in\mathcal{S}_0(\mathbb{R}^2)}$ admits a version that is a generalized centered real-valued Gaussian random field (see [12] for instance) and by (12), its covariance structure is given by

$$\mathbb{E}\left(\langle X,u\rangle\langle X,v\rangle\right) = \Re\left(\int_{\mathbb{R}^2}\widehat{u}(\xi)\overline{\widehat{v}(\xi)}f(\xi)\,d\xi\right)$$

for all $u, v \in \mathcal{S}_0(\mathbb{R}^2)$. Note that for any real-valued functions $u, v \in \mathcal{S}_0(\mathbb{R}^2)$, this covariance can be rewritten as

$$\mathbb{E}\left(\langle X,u\rangle\langle X,v\rangle\right) = \int_{\mathbb{R}^2}\widehat{u}(\xi)\overline{\widehat{v}(\xi)}f(\xi)\,d\xi \tag{7}$$

since the real-valued function f is even, and $\overline{\widehat{u}(\xi)} = \widehat{u}(-\xi)$ as well as $\overline{\widehat{v}(\xi)} = \widehat{v}(-\xi)$.

3. Monogenic signal of a random field

3.1. **Riesz transform.** The monogenic signal corresponds to the extension of the notion of 1D analytic signal to images [24], using a generalization of the Hilbert transform called the Riesz transform. The monogenic signal is defined as a combination of a real-valued function u defined on $\mathbb{R}^2$, which can be identified to an image, and its Riesz transform. Let us recall that the Riesz transform $\mathcal{R}u$ of a real-valued function $u \in L^2(\mathbb{R}^2)$ is the vector $\mathcal{R}u = \left(\mathcal{R}_1u, \mathcal{R}_2u\right) \in \mathbb{R}^2$ where for $k = 1, 2$

$$\mathcal{R}_ku(x) = \frac{1}{2\pi}\lim_{\varepsilon\to 0}\int_{\mathbb{R}^2\setminus B_\varepsilon(x)}\frac{x_k-y_k}{|x-y|^3}\,u(y)\,dy, \tag{8}$$

with $B_\varepsilon(x)$ the closed Euclidean ball with center x and radius ε. Note that we have

$$\forall\xi\in\mathbb{R}^2\setminus\{0\},\ \widehat{\mathcal{R}_ku}(\xi) = -i\frac{\xi_k}{|\xi|}\,\widehat{u}(\xi). \tag{9}$$

The following proposition presents useful properties of the Riesz transform [46, 41], including translation and dilation invariances.

Proposition 3.1. *For $k \in \{1,2\}$, $\mathcal{R}_k : L^2(\mathbb{R}^2) \to L^2(\mathbb{R}^2)$ is continuous. Moreover, for any real-valued functions $u, v \in L^2(\mathbb{R}^2)$,*

$$\langle\mathcal{R}_ku, v\rangle = -\langle u, \mathcal{R}_kv\rangle.$$

We also have

$$\mathcal{R}_1^2 + \mathcal{R}_2^2 = -I.$$

These last two properties imply that for any real-valued functions $u, v \in L^2(\mathbb{R}^2)$,

$$\langle\mathcal{R}u, \mathcal{R}v\rangle = \langle\mathcal{R}_1u, \mathcal{R}_1v\rangle + \langle\mathcal{R}_2u, \mathcal{R}_2v\rangle = \langle u, v\rangle.$$

In addition, $\mathcal{R}_k$ is translation and scale invariant, meaning that, for all $u \in L^2(\mathbb{R}^2)$, $x \in \mathbb{R}^2$, and $\lambda \in \mathbb{R}$

$$\mathcal{R}_k \tau_x u = \tau_x \mathcal{R}_k u, \quad \text{and} \quad \mathcal{R}_k d_\lambda u = d_\lambda \mathcal{R}_k u,$$

with

$$\tau_x u(y) = u(y-x) \quad \text{and} \quad d_\lambda u(y) = u(\lambda y). \tag{10}$$

The Riesz vector $\mathcal{R}X$ of a Gaussian random field X with harmonizable representation (2) can then be defined in the distribution sense, using the duality property.

Definition 3.2. *Let X be a real-valued Gaussian random field defined by (2). Then setting for any real-valued function $u \in \mathcal{S}_0(\mathbb{R}^2)$ and for $k = 1, 2$,*

$$\langle \mathcal{R}_k X, u \rangle = -\langle X, \mathcal{R}_k u \rangle,$$

the generalized random field $\mathcal{R}X$ is well-defined by

$$\mathcal{R}X(u) = \left(\langle \mathcal{R}_1 X, u \rangle, \langle \mathcal{R}_2 X, u \rangle \right), \ u \in \mathcal{S}_0(\mathbb{R}^2)$$

and called Riesz vector of the field X.

3.2. **Monogenic representation.** The monogenic signal is the combination, again in the distribution sense, of X and its Riesz vector $\mathcal{R}X$.

Definition 3.3. *Let X be a real-valued Gaussian random field defined by (2). The generalized random field $\mathcal{M}X$ with values in $\mathbb{R}^3$ defined by*

$$\mathcal{M}X(u) = \left(\langle X, u \rangle, \mathcal{R}X(u) \right), \ u \in \mathcal{S}_0(\mathbb{R}^2) \tag{11}$$

is then called monogenic signal of the random field X.

The monogenic signal $\mathcal{M}X$ of the Gaussian random field X is then a centered Gaussian vectorial generalized random field. Let us now state some of its properties.

Proposition 3.4. *Let X be a centered Gaussian random field with stationary increments and spectral density f, that is the random field defined by (2).*

(i) *The covariance function of the monogenic signal $\mathcal{M}X$ is given by: for any real-valued functions $u, v \in \mathcal{S}_0(\mathbb{R}^2)$,*

$$\mathcal{C}_{\mathcal{M}X}(u, v) = \mathbb{E}\left(\mathcal{M}X(u) \mathcal{M}X(v)^* \right) = \int_{\mathbb{R}^2} \widehat{u}(\xi) \overline{\widehat{v}(\xi)} f_{\mathcal{M}X}(\xi) d\xi, \tag{12}$$

where for a vector $h \in \mathbb{C}^3$, h^* denotes its conjugate transpose and where $f_{\mathcal{M}X}$ is defined as the complex matrix given for a.e. $\xi \in \mathbb{R}^2$ by

$$f_{\mathcal{M}X}(\xi) = \begin{pmatrix} 1 & -i\frac{\xi_1}{|\xi|} & -i\frac{\xi_2}{|\xi|} \\ i\frac{\xi_1}{|\xi|} & \frac{\xi_1^2}{|\xi|^2} & \frac{\xi_1 \xi_2}{|\xi|^2} \\ i\frac{\xi_2}{|\xi|} & \frac{\xi_1 \xi_2}{|\xi|^2} & \frac{\xi_2^2}{|\xi|^2} \end{pmatrix} f(\xi) = C_{\mathcal{M}}(\xi) f(\xi). \tag{13}$$

(ii) *Then, for any real-valued function $u \in \mathcal{S}_0(\mathbb{R}^2)$, $\langle X, u \rangle$ and the Riesz vector $\mathcal{R}X(u) = (\langle \mathcal{R}_1 X, u \rangle, \langle \mathcal{R}_2 X, u \rangle)$ are independent.*

(iii) *For any $x \in \mathbb{R}^2$, let the translation τ_x be defined by (10). Then for any real-valued function $u \in \mathcal{S}_0(\mathbb{R}^2)$, the random field $(\mathcal{M}X(\tau_x u))_{x \in \mathbb{R}^2}$ is a centered stationary vectorial Gaussian field with spectral density given by*

$$f_{\mathcal{M}X,u}(\xi) = f_{\mathcal{M}X}(\xi) |\widehat{u}(\xi)|^2 \text{ for a.e. } \xi \in \mathbb{R}^2, \tag{14}$$

where $f_{\mathcal{M}X}$ is defined in (13).

(iv) *Let $u \in \mathcal{S}_0(\mathbb{R}^2)$ be a real-valued function and for any integer $j \in \mathbb{Z}$, consider the real-valued function $u_j : \mathbb{R}^2 \to \mathbb{R}$ defined by*

$$u_j(x) = 2^{-j} u(2^{-j} x). \tag{15}$$

If the spectral density f is homogeneous of order $H \in (0, 1)$, i.e. is defined by (3), then for any $j \in \mathbb{Z}$,

$$(\mathcal{M}X(\tau_x u_j))_{x \in \mathbb{R}^2} \overset{d}{=} 2^{j(H+1)} (\mathcal{M}X(\tau_{2^{-j}x} u))_{x \in \mathbb{R}^2}.$$

Proof. See Appendix. □

Remark 3.5. *The symbol j is associated to a notion of scale, introducing a multiscale perspective to field analysis. This approach allows for the deployment of a strategy to estimate various characteristics. Indeed, as we will see in the numerical section, extracting monogenic coefficients at different scales provides a framework for numerical estimation.*

When X is a lighthouse random field and when u is radial, next proposition gives the marginal distribution of $\mathcal{M}X(u)$: its components are in particular independent.

Proposition 3.6. *Let $(H,\delta) \in (0,1)\times(0,\pi/2]$ and let X be the lighthouse random field with spectral density $f_{H,\delta}$ introduced by Definition 2.1. If the real-valued function $u \in \mathcal{S}_0\left(\mathbb{R}^2\right)$ is radial, then for all $x \in \mathbb{R}^2$,*

$$\mathcal{M}X(\tau_x u) \overset{d}{=} \sqrt{c_X(u)} D_\delta Z,$$

with Z a standard Gaussian vector with values in $\mathbb{R}^3$,

$$c_X(u) = \mathrm{Var}(\langle X, u\rangle) = \int_{\mathbb{R}^2} |\widehat{u}(\xi)|^2 f_{H,\delta}(\xi) d\xi,$$

and the diagonal matrix

$$D_\delta = \mathrm{diag}\left(1, \sqrt{\frac{1}{2} + \frac{\sin(2\delta)}{4\delta}}, \sqrt{\frac{1}{2} - \frac{\sin(2\delta)}{4\delta}}\right).$$

Proof. See Appendix. □

Let us now consider the spherical coordinates of the monogenic signal $\mathcal{M}X$. For any $u \in \mathcal{S}_0(u)$, let us write

$$\mathcal{M}X(u) = A_X(u)\vec{v}_X(u) \tag{16}$$

with $A_X(u) = |\mathcal{M}X(u)|$, the amplitude and

$$\vec{v}_X(u) = \begin{pmatrix} \cos(\varphi_X(u)) \\ \sin(\varphi_X(u))\cos(\theta_X(u)) \\ \sin(\varphi_X(u))\sin(\theta_X(u)) \end{pmatrix} \in S^2 \tag{17}$$

with $\varphi_X(u) \in [0,\pi)$, the phase, and $\theta_X(u) \in [-\pi,\pi)$, the orientation.

The main interest of the monogenic signal comes from the strong relation between the values of its phase and the geometrical structure of the local signal variations. Moreover, the amplitude is invariant by rotation. When the random field X is a lighthouse field, next proposition gives the spherical coordinates' densities.

Theorem 3.7. *Let $(H,\delta) \in (0,1)\times(0,\pi/2]$ and let X be the lighthouse field with spectral density $f_{H,\delta}$ given by (5). Let the generalized random field $(A_X, \varphi_X, \theta_X)$ be the spherical coordinates of the monogenic signal $\mathcal{M}X$, i.e. be defined by (16). Let $u \in \mathcal{S}_0\left(\mathbb{R}^2\right)$ be a non zero radial function.*

(i) *Then $(A_X(\tau_x u), \varphi_X(\tau_x u), \theta_X(\tau_x u))_{x\in\mathbb{R}^2}$, with τ_x defined by (10), is a stationary random field.*

(ii) *The random orientation $\theta_X(u)$ follows an offset normal distribution whose probability density function is defined on $[-\pi,\pi)$ by*

$$\theta \mapsto \frac{\sqrt{1-\chi_X(u)^2}}{2\pi(1-\chi_X(u)\cos(2\theta))},$$

with

$$\chi_X(u) = \frac{\sin(2\delta)}{2\delta}. \tag{18}$$

(iii) *Moreover, with $c_X(u)$ and D_δ defined in Proposition 3.6,*

$$A_X(u)^2 \overset{d}{=} c_X(u) A_\delta^2$$

with $A_\delta^2 = |D_\delta Z|^2$ for $Z \sim \mathcal{N}(0, I_3)$ that follows a generalized chi-square distribution $\mathbb{E}\left(A_\delta^2\right) = 2$.

(iv) *In the isotropic case, if $\delta = \pi/2$, $\theta_X(u)$ follows a uniform distribution on $(-\pi,\pi)$ and is independent of $(A_X(u), \varphi_X(u))$. Moreover, the density function of the phase $\varphi_X(u)$ is given by*

$$\phi \mapsto \frac{\sin(\phi)}{(1+\sin^2(\phi))^{3/2}} \mathbf{1}_{(0,\pi)}(\phi).$$

(v) *Let $j \in \mathbb{Z}$ and let u_j be defined by (15). Then,*

$$\vec{v}_X(u_j) \overset{d}{=} \vec{v}_X(u),$$

and so the distribution of $\vec{v}_X(u_j)$ does not depend on j. Moreover,

$$A_X(u_j) \overset{d}{=} 2^{j(H+1)} A_X(u).$$

Remark 3.8. *The parameter $\chi_X(u)$ that characterizes the distribution of the orientation $\theta_X(u)$ does not depend on $u \in \mathcal{S}_0(\mathbb{R}^2)$. Moreover, this parameter is the so called coherence index, see [40], of the lighthouse field X. It allows to measure the directional anisotropy, see section 6.2 which proposes an estimator of this index.*

Proof. See Appendix. □

The next section is devoted to the numerical approach and in particular allows to illustrate the previous proposition.

4. Simulation

4.1. **Simulation of lighthouse random fields.**

All realizations of lighthouse random fields presented in this paper have been simulated using a turning-band method adapted to generate two-dimensional anisotropic fractional Brownian fields [14]. This procedure is based on the simulation of several independent one-dimensional processes, each one generated on an oriented band passing through a given origin. Once generated, these processes are linearly combined to build the desired two-dimensional field. This method produces one random field realization, an image, on a grid $\mathcal{G}_N = \{0, \dots, N-1\} \times \{0, \dots, N-1\}$ of size $N \times N$. Examples of lighthouse random field realizations are presented in Figure 1, for $H = 0.5$ and for $\delta = \pi/2$, $\pi/4$, $\pi/12$ and $\pi/64$, with $N = 1024$.

4.2. **Computation of the monogenic signal.**

Following Equation (11), from a realization of a lighthouse random field of size $N \times N$, one can compute the associated monogenic signal. As we noted in Remark 3.5 following Proposition 3.4, we consider monogenic analysis with a multiscale method. Defining monogenic wavelet transforms is a recent topic. The main idea is to combine parallel filterbanks $(H_j, G_j)_{j\in\mathbb{Z}}$ whose underlying wavelet functions form a Riesz triple. We propose to use the undecimated filterbank design, like in [35] for the numerical scheme and in [30] for the Hurst estimation, because it allows for translation invariance in the numerical scheme as well as interscale connection.

At a given scale, the monogenic signal is of size $N \times N \times 3$ and consists of a filtered version of the realization and both Riesz transforms of the filtered realization.

The essential action of the Riesz transform is a pure phase-shifting operation, consequently the low-pass and high-pass filters H_1 and G_1 are required to be perfectly neutral with respect to the signal's phase. Their frequency response must then be radial, positive and real-valued. In the following, we propose to use the filter G_1, defined on the frequency domain $\widehat{\mathcal{G}}_N = \{-\frac{N}{2}, \dots, \frac{N}{2}-1\} \times \{-\frac{N}{2}, \dots, \frac{N}{2}-1\}$ as

$$\forall \xi \in \widehat{\mathcal{G}}_N, \quad \widehat{G}_1(\xi) = 1 - e^{-|2\pi\xi|^2/2}.$$

This high-pass filter has proven particularly efficient to define a monogenic representation of colored images in [45]. Figure 2 displays the filter G_1 in the frequency domain and the corresponding low-pass filter H_1, defined for all $\xi \in \widehat{\mathcal{G}}_N$ by $\widehat{H}_1(\xi) = \sqrt{1 - \widehat{G}_1(\xi)^2}$. In this case, the filterbank is computed in the frequency domain with linear complexity, using the 2-dimensional Fast Fourier Transform.

As we mentioned earlier, a multiscale decomposition of the monogenic signal is required in our estimation procedure, presented in the next sections. To this end, we propose to use an undecimated filterbank, associated with the filter G_1 and the dilated versions

$$\forall j \geq 2, \quad \forall \xi \in \widehat{\mathcal{G}}_N, \quad \widehat{G}_j(\xi) = \widehat{G}_1(2^{j-1}\xi), \quad \text{and} \quad \widehat{H}_j(\xi) = \sqrt{1 - \widehat{G}_j(\xi)^2}.$$

In Figure 2, we also present the templates of the filters for the next scale 2. As the bank of filters is undecimated, the realization remains on the same grid $\mathcal{G}_N$ at any scale j. The main advantage of this is information redundancy, that is shown to improve inference by decreasing the variance of the estimates. The choice of the optimal scale is a classic problem and is regularly discussed in articles using wavelet decomposition. For example, it is known that there is a bias-variance trade-off for choosing scales: the selection of small scale increases the bias, but decrease the variance of the estimator. This choice results from a compromise, which we propose in this paper.

In practice, given an image I_j of size $N \times N$ at scale $j \geq 0$, the monogenic signal is obtained by applying the high-pass filter G_j to I_j and then by computing both Riesz transforms $\mathcal{R}_1 I_j, \mathcal{R}_2 I_j$ on the filtered realization in the spectral domain. Then the monogenic signal at scale j is given by these 3 images $I_j, \mathcal{R}_1 I_j, \mathcal{R}_2 I_j$ of size $N \times N$ seen as an image of size $N \times N$ with vectorial values in $\mathbb{R}^3$. The spherical coordinates at each pixel yield the monogenic parameters A_j, φ_j, θ_j of amplitude, phase and orientation as threw new images of size $N \times N$. The realization, I_{j+1}, at scale $j+1$ is determined by applying the low-pass filter H_j to I_j.

Hence from I_0 the realization of our random field X on the discrete grid $\mathcal{G}_N$ we consider for $j \geq 1$ the filtered image I_j as a realization of $\{\langle X, \tau_x u_j\rangle; x \in \mathcal{G}_N\}$ and its Riesz transforms $\mathcal{R}_k I_j$ as a realization of $\{\langle \mathcal{R}_k X, \tau_x u_j\rangle; x \in \mathcal{G}_N\}$, while the monogenic parameters $(A_j, \varphi_j, \theta_j)$ are seen as a realization of $\{(A_X(\tau_x u_j), \varphi_X(\tau_x u_j), \theta_X(\tau_x u_j)); x \in \mathcal{G}_N\}$. Note that the choice of G_1 and H_1 ensures that we may assume that u is a radial function satisfying the moment condition $D^j \widehat{u}(0) = 0$ for $|j| = j_1 + j_2 \leq 1$.

Figure 3 illustrates Theorem 3.7: it presents the empirical and theoretical probability density functions of the amplitude, the orientation and the phase of the monogenic signal, for a given lighthouse field of parameters $H = 0.5$ and $\delta = \pi/2$, $\pi/3$ or $\pi/6$. The realization used for this estimation is of size 1024×1024 and we apply the filter G_1 presented above. To avoid border artefacts we remove 15% on each side of the images of monogenic parameters. Notice how, thanks to the stationarity, one realization is sufficient to provide satisfying empirical distributions for the amplitude, the phase and the orientation of the monogenic signal.

A MATLAB implementation (`https://github.com/claunay/monog\_img`) is available online for simulating lighthouse random fields and their monogenic signal, and for estimating their parameters (H, δ).

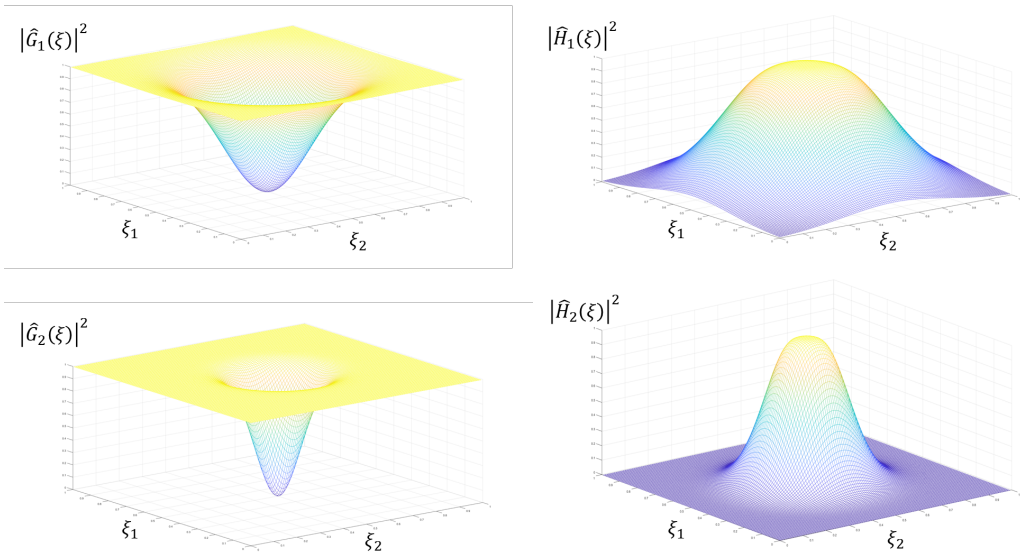

FIGURE 2. The high-pass filter G_1 and the associated low-pass filter H_1 at scale 1 and the high-pass filter G_2 and the associated low-pass filter H_2 at scale 2 presented here in the frequency domain, are used in the monogenic representation of lighthouse random fields.

5. Inference based on the monogenic signal

5.1. Monogenic tensor.

Definition 5.1. *Let X be the random field associated to the spectral density f by (2) and $u \in \mathcal{S}_0\left(\mathbb{R}^2\right)$. Then, the monogenic tensor of the Gaussian random vector $\mathcal{M}X(u)$ is its covariance matrix*

$$\mathcal{T}_{\mathcal{M}X}(u) := \mathbb{E}\left(\mathcal{M}X(u)\mathcal{M}X(u)^*\right) \in \mathcal{M}_3(\mathbb{R}).$$

When X is the lighthouse field with spectral density $f_{H,\delta}$, by Proposition 3.6, the monogenic tensor of a radial function $u \in \mathcal{S}_0\left(\mathbb{R}^2\right)$ is simply the diagonal matrix

$$\mathcal{T}_{\mathcal{M}X}(u) = c_X(u)\mathrm{diag}\left(1, \frac{1}{2} + \frac{\sin(2\delta)}{4\delta}, \frac{1}{2} - \frac{\sin(2\delta)}{4\delta}\right)$$

In view of Theorem 3.7, for $u \in \mathcal{S}_0\left(\mathbb{R}^2\right)$ a radial function, for any scale j, we now consider the monogenic tensor of the function u_j defined by (15)

$$\mathcal{T}_{\mathcal{M}X}(u_j) := \mathbb{E}\left(\mathcal{M}X(u_j)\mathcal{M}X(u_j)^*\right) \in \mathcal{M}_3(\mathbb{R}).$$

Since X is the lighthouse field with spectral density $f_{H,\delta}$, we have

$$\mathcal{T}_{\mathcal{M}X}(u_j) = \int_{\mathbb{R}^2} f_{\mathcal{M}X,u_j}(\xi)d\xi = 2^{2j(H+1)} \int_{\mathbb{R}^2} f_{\mathcal{M}X,u}(\xi)d\xi$$

where the spectral densities $f_{\mathcal{M}X,u_j}$ and $f_{\mathcal{M}X,u}$ are given by (14). This scaling property will lead to an estimator of the Hurst index H after estimating the monogenic tensors $\mathcal{T}_{\mathcal{M}X}(u_j)$ for each scale j. A natural empirical estimator of $\mathcal{T}_{\mathcal{M}X}(u_j)$ is then given by

$$\mathcal{T}M_j^{\mathrm{emp}} = \frac{1}{N^2} \sum_{x \in \mathcal{G}_N} \mathcal{M}X(\tau_x u_j)\mathcal{M}X(\tau_x u_j)^*, \tag{19}$$

where we recall that $\mathcal{G}_N = \{0, \ldots, N-1\}^2$ is the grid of size N^2 on which the random field X is observed.

Let us emphasize that in the sequel, each symmetric matrix $M = (m_{\ell\ell'})_{1 \le \ell, \ell' \le 3}$ of size 3×3 is identified, when stating asymptotic normality property, with the vector of length 6, $(m_{11}, m_{22}, m_{33}, m_{12}, m_{13}, m_{23})$. We obtain the following theorem.

Theorem 5.2. *Let $(H, \delta) \in (0,1) \times (0, \pi/2]$ and let X be the lighthouse field with spectral density $f_{H,\delta}$ given by (5). Let $u \in \mathcal{S}_0\left(\mathbb{R}^2\right)$ be a non-zero radial function and let $j \in \mathbb{Z}$. Then $\mathcal{T}M_j^{emp}$ is an unbiased estimator of the monogenic tensor $\mathcal{T}_{\mathcal{M}X}(u_j)$ and*

$$\mathcal{T}M_j^{emp} \xrightarrow[N \to \infty]{a.s.} \mathcal{T}_{MX}(u_j). \tag{20}$$

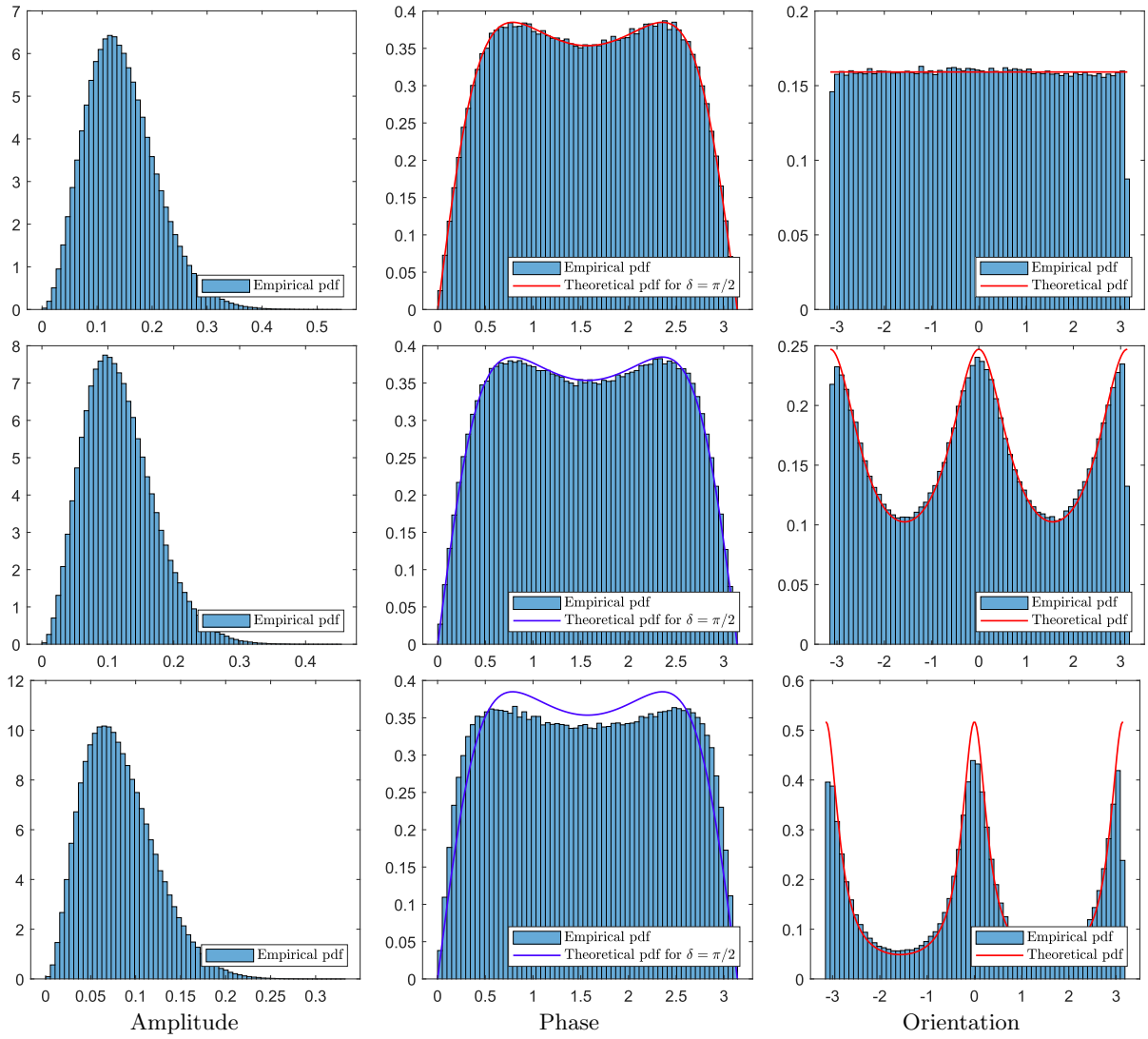

FIGURE 3. Empirical probability density functions of the amplitude, phase and orientation of the monogenic signal of a lighthouse fields with parameters $H = 0.5$ and $\delta = \pi/2$ (top), $\delta = \pi/3$ (middle), $\delta = \pi/6$ (bottom), computed on one realization of size 1024×1024

.

In addition, for $H < 1/2$ *or choosing* $u \in \mathcal{S}_1(\mathbb{R}^2)$ *for* $1/2 \leq H < 1$*, there exists a symmetric non-negative matrix* $\Gamma_{\mathcal{T}M}(u_j) \in \mathcal{M}_6(\mathbb{R})\backslash\{0\}$ *such that*

$$N\left(\mathcal{T}M_j^{emp} - \mathcal{T}_{\mathcal{M}X}(u)\right) \xrightarrow[N\to\infty]{d} \mathcal{N}\left(0, \Gamma_{\mathcal{T}M}(u_j)\right).$$

Proof. See Appendix. □

By using spherical coordinates (16), we can also write

$$\mathcal{T}_{\mathcal{M}X}(u_j) = \mathbb{E}\left(A_X(u_j)^2 \vec{v}_X(u_j)\vec{v}_X(u_j)^*\right).$$

Therefore, since $\mathrm{Tr}\left(\vec{v}_X(u_j)\vec{v}_X(u_j)^*\right) = |\vec{v}_X(u_j)|^2 = 1$,

$$\mathrm{Tr}\left(\mathcal{T}_{\mathcal{M}X}(u_j)\right) = \mathbb{E}\left(A_X(u_j)^2 \mathrm{Tr}\left(\vec{v}_X(u_j)\vec{v}_X(u_j)^*\right)\right) = \mathbb{E}\left(A_X(u_j)^2\right).$$

Then as a simple consequence of Theorem 5.2, we can propose the following consistent asymptotically normal estimator of $\mathbb{E}\left(A_X(u_j)^2\right)$.

Corollary 5.3. *Let $(H,\delta) \in (0,1)\times(0,\pi/2]$ and let X be the lighthouse field with spectral density $f_{H,\delta}$ given by (5). Let $u \in \mathcal{S}_0\left(\mathbb{R}^2\right)$ be a non-zero radial function and let $j \in \mathbb{Z}$. Then*

$$V_j^{emp} := \mathrm{Tr}\left(\mathcal{T} M_j^{emp}\right) = \frac{1}{N^2}\sum_{x\in\mathcal{G}_N} |\mathcal{M}X(\tau_x u_j)|^2 \tag{21}$$

is an unbiased estimator of $\mathbb{E}\left(A_X(u_j)^2\right)$ and

$$V_j^{emp} \xrightarrow[N\to\infty]{a.s.} \mathbb{E}\left(A_X(u_j)^2\right).$$

Moreover for $H<1/2$ or choosing $u\in\mathcal{S}_1\left(\mathbb{R}^2\right)$ when $1/2\le H<1$, there exists $\sigma^2(u_j)>0$ such that

$$N\left(V_j^{emp} - \mathbb{E}\left(A_X(u_j)^2\right)\right) \xrightarrow[N\to\infty]{d} \mathcal{N}\left(0,\sigma^2(u_j)\right).$$

In addition, if $\widehat{u}_j$ has support in $\mathbb{T}^2$, then

$$\sigma^2(u_j) = 32\pi^2 \int_{\mathbb{T}^2} |\widehat{u}_j(\xi)|^4 f_{H,\delta}(\xi)^2 d\xi.$$

Proof. See Appendix. □

Now using the fact that $A_X(u_j)^2 \overset{d}{=} 2^{2j(H+1)} A_X(u)^2$, by Theorem 3.7, the amplitudes of the monogenic signal at each scale provide an estimator of the random field Hurst index, introduced in next section.

5.2. **Estimation of the Hurst index.** Since

$$\frac{\mathbb{E}\left(A_X(u_{j+1})^2\right)}{\mathbb{E}\left(A_X(u_j)^2\right)} = \frac{2^{2(j+1)(H+1)}\mathbb{E}\left(A_X(u)^2\right)}{2^{2j(H+1)}\mathbb{E}\left(A_X(u)^2\right)} = 2^{2H+2}, \tag{22}$$

we simply propose

$$H_j^{\mathrm{emp}} = \frac{1}{2\log(2)}\log\left(\frac{V_{j+1}^{\mathrm{emp}}}{V_j^{\mathrm{emp}}}\right) - 1. \tag{23}$$

as an estimator of the Hurst index H.

Theorem 5.4. *Let $(H,\delta)\in(0,1)\times(0,\pi/2]$ and let X be the lighthouse field with spectral density $f_{H,\delta}$ given by (5). Let $u\in\mathcal{S}_0\left(\mathbb{R}^2\right)$ be a non-zero radial function and let $j\in\mathbb{Z}$. Then recalling (23)*

$$H_j^{emp} \xrightarrow[N\to\infty]{a.s.} H.$$

Let now $H<1/2$ or let $u\in\mathcal{S}_1(\mathbb{R}^2)$ when $1/2\le H<1$. Then there exists $\rho(u_j)\ge 0$ such that

$$N\left[\begin{pmatrix} V_j^{emp} \\ V_{j+1}^{emp}\end{pmatrix} - \begin{pmatrix} \mathbb{E}\left(A_X(u_j)^2\right) \\ \mathbb{E}\left(A_X(u_{j+1})^2\right)\end{pmatrix}\right] \xrightarrow[N\to\infty]{d} \mathcal{N}\left(0, \begin{pmatrix} \sigma^2(u_j) & \rho(u_j) \\ \rho(u_j) & \sigma^2(u_{j+1})\end{pmatrix}\right),$$

with $\sigma^2(u_j)$ and $\sigma^2(u_{j+1})$ given by Corollary 5.3. Moreover

$$N\left(H_j^{emp} - H\right) \xrightarrow[N\to\infty]{d} \mathcal{N}\left(0,\gamma^2(u_j)\right),$$

with

$$\gamma^2(u_j) = \frac{2^{4H+4}\sigma^2(u_j) - 2^{2H+3}\rho(u_j) + \sigma^2(u_{j+1})}{\left(2\log(2)\mathbb{E}\left(A_X(u_{j+1})^2\right)\right)^2}. \tag{24}$$

In addition, if $\widehat{u}_j$ has support in $\mathbb{T}^2$, then we also have

$$\gamma^2(u_j) = \frac{2\pi^2}{\left(\log(2)c_X(u_{j+1})\right)^2}\int_{\mathbb{R}^2}\left(|\widehat{u}_{j+1}(\xi)|^2 - 2^{2H+2}|\widehat{u}_j(\xi)|^2\right)^2 f_{H,\delta}(\xi)^2 d\xi.$$

Proof. See Appendix. □

Figure 4 and Table 1 present the performances of this strongly consistent estimator of the Hurst index. In order to compare the performances of the estimation method presented with other standard estimation methods in Section 6.3, we use the same simulation settings as in [25]. The synthesized textures, realizations of lighthouse fields, are of size 1024×1024. Note that the multiscale decomposition creates border artefacts: at each scale, pixels at the border of the image degrade the quality of the estimation. To improve the results, we remove a given percentage of pixels on each side of the realizations. In our experiments, we choose to remove 15% of pixels on each side of the realizations such that the size of the grid is given by $N=719$. Figure 4a) presents the estimates of the logarithm of monogenic signal squared amplitude computed at each scale, on one realization of a lighthouse random field with parameters $\delta=\pi/4$ and $H=0.5$. We observe a good linearity except at first and last scales. Scales 3 and 4 provide an estimate of the slope, whose corresponding line is displayed through the red dotted line, while the one with theoretical slope given by

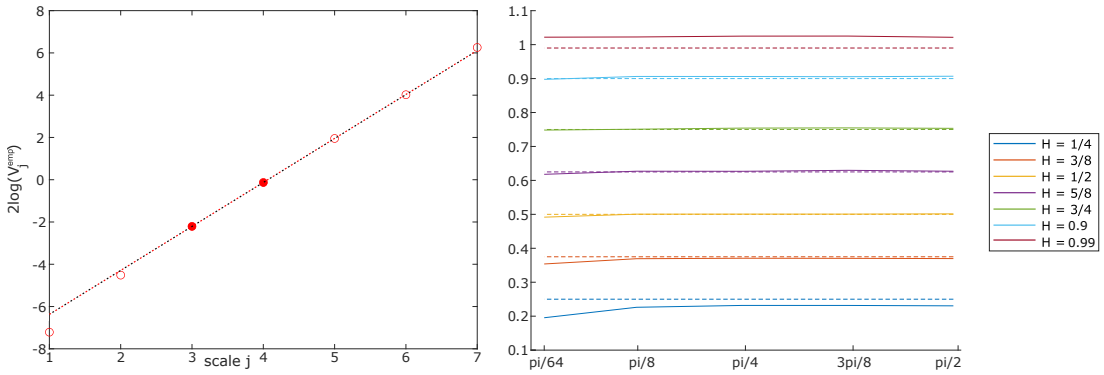

a) $\log(V_j^{\text{emp}})$ for $H = 0.5$ and $\delta = \pi/4$ b) Empirical mean of H_3^{emp}

FIGURE 4. Estimation of H for an initial simulation of size 1024×1024 (a) Logarithm of V_j^{emp} with respect to the scale j computed on one realization with $H = 0.5$ and $\delta = \pi/4$. Dotted lines are computed using two scales ($j = 3, 4$), with empirical slope in red and with theoretical slope in black. (b) Empirical mean of H_3^{emp} (solid lines) given by (23), computed on 300 Monte-Carlo simulations for $H \in \left\{\frac{1}{4}, \frac{3}{8}, \frac{1}{2}, \frac{5}{8}, \frac{3}{4}, 0.9, 0.99\right\}$ (dotted lines) and $\delta \in \left\{\frac{\pi}{64}, \frac{\pi}{8}, \frac{\pi}{4}, \frac{3\pi}{8}, \frac{\pi}{2}\right\}$.

	H	$\delta = \pi/2$	$\delta = 3\pi/8$	$\delta = \pi/4$	$\delta = \pi/8$	$\delta = \pi/64$
MSE						
	0.3	0.0002	0.0002	0.0003	0.0007	0.0034
	0.5	0.0001	0.0002	0.0002	0.0004	0.0023
	0.7	0.0001	0.0002	0.0003	0.0005	0.0024
	0.8	0.0001	0.0002	0.0003	0.0005	0.0025
	0.9	0.0002	0.0002	0.0003	0.0005	0.0027
	0.99	0.0017	0.0022	0.0024	0.0026	0.0050
Variance						
	0.3	0.0001	0.0001	0.0002	0.0005	0.0022
	0.5	0.0001	0.0002	0.0002	0.0004	0.0023
	0.7	0.0001	0.0002	0.0002	0.0004	0.0024
	0.8	0.0001	0.0002	0.0002	0.0005	0.0025
	0.9	0.0001	0.0002	0.0003	0.0005	0.0027
	0.99	0.0007	0.0010	0.0012	0.0015	0.0039

TABLE 1. Mean square error and empirical variance of the estimates H_3^{emp}, computed on 300 Monte-Carlo simulations of size 1024×1024.

the real value of H is provided by the black dotted line. This example shows how, in practice, using the first scales ($j = 1, 2$) and the deepest scales ($j \geq 7$) of the analysis would impair the estimation.

These observations are coherent with several numerical studies on multiscale representation of images [48]. The first scales seem to be noisy since we simulate a field that has a spectrum which is a uniform power-law over almost the full range of frequency. This property will be unsuitable for numerical simulation at very high frequencies, frequencies associated with the initial scales of the decomposition. On the contrary, information given by the deepest scales is limited by strong border artefacts and by the size of the filters used for the multi-scale decomposition. Indeed, although the decomposition is not decimated, the filters are dilated, making artifacts due to edge effects increasingly visible.

Then we choose H_3^{emp} given by Equation (23) as estimator of H. We consider 300 Monte-Carlo simulations. Figure 4b) presents the empirical mean of Hurst index estimates for $H \in \{\frac{1}{4}, \frac{3}{8}, \frac{1}{2}, \frac{5}{8}, \frac{3}{4}, 0.9, 0.99\}$ (color) and degrees of anisotropy $\delta \in \{\frac{\pi}{64}, \frac{\pi}{8}, \frac{\pi}{4}, \frac{3\pi}{8}, \frac{\pi}{2}\}$ (x-axis). The true Hurst index for each degree of anisotropy is displayed as a dotted line. Table 1 provides the mean squared error between these estimates and the true Hurst index, and the empirical variance of the 300 estimates. These results illustrate the high performance of this estimator and stability with respect to anisotropy, especially when H is distant from 0 or 1 and δ larger than $\pi/8$. In addition, for a given H, the greatest δ is, the more efficient the estimator is. In Section 6.3 below, this estimator based on the monogenic signal will be compared with one based on the Riesz structure tensor and estimators proposed in [44, 25] in the isotropic framework (that is when $\delta = \pi/2$).

In the following, we recall the definition of the structure tensor, based only on the Riesz transform, that has previously been used for Hurst index estimation [37, 40]. We show that, as the monogenic tensor, it can provide strongly consistent estimators for the Hurst index as well as for the degree of anisotropy. Then we compare both Hurst index estimators numerically.

6. Inference using the structure tensor

6.1. **Riesz structure tensor.** Olhede et al. [37] and Polisano et al. [40] propose to use the Riesz structure tensor to detect the directionality and anisotropy of random fields.

Definition 6.1. *Let X be a real valued Gaussian random field defined by (2). Then for any $u \in \mathcal{S}_0\left(\mathbb{R}^d\right)$, the Riesz structure tensor is the matrix*

$$J_X(u) := \mathbb{E}\left(\mathcal{R}X(u)\mathcal{R}X(u)^*\right).$$

Note that we simply have

$$\mathcal{T}M_X(u) = \begin{pmatrix} c_X(u) & 0 \\ 0 & J_X(u) \end{pmatrix}.$$

Choosing $u \in \mathcal{S}_0\left(\mathbb{R}^2\right)$ a radial function, for any scale j, we consider now the Riesz structure tensor

$$J_X(u_j) := \mathbb{E}\left(\mathcal{R}X(u_j)\mathcal{R}X(u_j)^*\right).$$

Note that when X is the lighthouse field with spectral density $f_{H,\delta}$, by Proposition 3.6, this Riesz structure tensor is simply the diagonal matrix

$$J_X(u_j) = c_X(u)\mathrm{diag}\left(\frac{1}{2} + \frac{\sin(2\delta)}{4\delta}, \frac{1}{2} - \frac{\sin(2\delta)}{4\delta}\right)$$

Moreover, given a realization of an elementary field defined on the grid $\mathcal{G}_N$ of size $N \times N$, at each scale, an empirical estimator of the structure tensor is

$$J_j^{\mathrm{emp}} = \frac{1}{N^2}\sum_{x\in\mathcal{G}_N} \mathcal{R}X\left(\tau_x u_j\right)\mathcal{R}X\left(\tau_x u_j\right)^* = \left[\mathcal{T}M_j^{\mathrm{emp}}\right]_{2\le p,q\le 3}. \tag{25}$$

We obtain the following proposition. As done when studying the monogenic tensor, in the sequel, each symmetric matrix $M = (m_{\ell\ell'})_{1\le\ell,\ell'\le 2}$ of size 2×2 is identified, when stating asymptotic normality property, with the vector (m_{11}, m_{22}, m_{12}) of length 3.

Proposition 6.2. *Let $(H,\delta) \in (0,1)\times(0,\pi/2]$ and let X be the lighthouse field with spectral density $f_{H,\delta}$ given by (5). Let $u \in \mathcal{S}_0\left(\mathbb{R}^2\right)$ be a non-zero radial function and let $j \in \mathbb{Z}$. Then J_j^{emp} is an unbiased estimator of $J_X(u_j)$ and*

$$J_j^{emp} \xrightarrow[N\to\infty]{a.s.} J_X(u_j). \tag{26}$$

Moreover, for $H < 1/2$ or choosing $u \in \mathcal{S}_1(\mathbb{R}^2)$ for $1/2 \le H < 1$, there exists a symmetric non negative matrix $\Gamma_{\mathcal{R}}(u_j) \in \mathcal{M}_3(\mathbb{R})\backslash\{0\}$ such that

$$N\left(J_j^{emp} - J_X(u_j)\right) \xrightarrow[N\to\infty]{d} \mathcal{N}\left(0, \Gamma_{\mathcal{R}}(u_j)\right).$$

Proof. See Appendix. □

6.2. **Estimation of the coherence index.**

Let us now recall the definition of the coherence index of the structure tensor $\mathcal{R}X(u)$.

Definition 6.3. *Let X be a real valued Gaussian random field defined by (2) and let $u \in \mathcal{S}_0\left(\mathbb{R}^d\right)$. Then if the Riesz structure tensor $J_X(u) \neq 0$, its coherence index is*

$$\chi_X(u) = \frac{\lambda^+(u) - \lambda^-(u)}{\lambda^+(u) + \lambda^-(u)} \in [0,1)$$

where $\lambda^+(u)$ and $\lambda^-(u)$ denote respectively the largest and the smallest eigenvalue of the non-negative symmetric matrix $J_X(u)$.

Considering now the multi-scale approach, for each scale j, we still denote by $\lambda^+(u_j)$ the largest eigenvalue of the Riesz tensor $J_X(u_j)$ and by $\lambda^-(u_j)$ its smallest eigenvalue. Then the coherence index, see [40], given by

$$\chi_X(u_j) = \frac{\lambda^+(u_j) - \lambda^-(u_j)}{\lambda^+(u_j) + \lambda^-(u_j)} \in [0,1), \tag{27}$$

allows to measure the directional anisotropy.

Consider now a lighthouse field X of parameters $(H,\delta) \in (0,1)\times(0,\pi/2]$ and assume that u is a non zero radial function. Then, since by Proposition 3.6

$$\mathcal{T}M_X(u_j) = \begin{pmatrix} c_X(u_j) & 0 \\ 0 & J_X(u_j) \end{pmatrix},$$

we simply get

$$\lambda^{\pm}(u_j) = c_X(u_j) \times \left[\frac{1}{2} \pm \frac{\sin(2\delta)}{4\delta}\right] > 0$$

as in Polisano et al. [40]. Moreover,

$$\lambda^{\pm}(u_j) = 2^{j(2H+2)}\lambda^{\pm}(u). \tag{28}$$

In addition, the coherence index of the structure tensor at scale j does not depend on the considered scale, but only on the anisotropic parameter δ:

$$\chi_X(u_j) = \frac{\sin(2\delta)}{2\delta}. \tag{29}$$

The case $\delta = \frac{\pi}{2}$, corresponding to the isotropic one yields $\chi_X(u_j) = 0$. As δ decreases, the lighthouse field becomes more directionally oriented and the coherence index is growing to 1.

With the aim to estimate the coherence index $\chi_X(u_j)$, we first estimate the eigenvalues $\lambda^+(u_j)$ and $\lambda^-(u_j)$, respectively by $\lambda_j^{+\text{emp}}$ the largest eigenvalue of the matrix J_j^{emp} and $\lambda_j^{-\text{emp}}$ its smallest eigenvalue. We obtain the following proposition.

Proposition 6.4. *Let $(H,\delta) \in (0,1)\times(0,\pi/2]$ and let X be the lighthouse field with spectral density $f_{H,\delta}$ given by (5). Let $u \in \mathcal{S}_0\left(\mathbb{R}^2\right)$ be a non-zero radial function and let $j \in \mathbb{Z}$. Then*

$$\lambda_j^{\pm emp} \xrightarrow[N\to\infty]{a.s.} \lambda_j^{\pm}.$$

Moreover, for $H < 1/2$ or choosing $u \in \mathcal{S}_1(\mathbb{R}^2)$ for $1/2 \le H < 1$,

$$N\left(\begin{pmatrix}\lambda_j^{+emp}\\ \lambda_j^{-emp}\end{pmatrix} - \begin{pmatrix}\lambda^+(u_j)\\ \lambda^-(u_j)\end{pmatrix}\right) \xrightarrow[N\to+\infty]{d} \mathcal{N}(0, [\Gamma_{\mathcal{R}}(u_j)]_{1\le l,l'\le 2}).$$

In addition, assuming that $\widehat{u}_j$ has support in $\mathbb{T}^2$, one has for $1 \le l, l' \le 2$

$$[\Gamma_{\mathcal{R}}(u_j)]_{l,l'} = 8\pi^2 \int_{\mathbb{T}^2} \frac{\xi_l^2\xi_{l'}^2}{|\xi|^4} |\widehat{u}_j(\xi)|^4 f_{H,\delta}(\xi)^2 d\xi.$$

Proof. See Appendix. □

Now for each integer j, we define

$$\chi_X(u_j)^{\text{emp}} = \frac{\lambda_j^{+\text{emp}} - \lambda_j^{-\text{emp}}}{\lambda_j^{+\text{emp}} + \lambda_j^{-\text{emp}}}, \tag{30}$$

as estimator of the coherence index for the scale j.

Theorem 6.5. *Let $(H,\delta) \in (0,1)\times(0,\pi/2]$ and let X be the lighthouse field with spectral density $f_{H,\delta}$ given by (5). Let $u \in \mathcal{S}_0\left(\mathbb{R}^2\right)$ be a non-zero radial function and let $j \in \mathbb{Z}$. Then*

$$\chi_X(u_j)^{emp} \xrightarrow[N\to\infty]{a.s.} \chi_X(u_j).$$

Moreover, for $H < 1/2$ or choosing $u \in \mathcal{S}_1(\mathbb{R}^2)$ for $1/2 \le H < 1$, one has

$$N\left(\chi_X(u_j)^{emp} - \chi_X(u_j)\right) \xrightarrow[N\to+\infty]{d} \mathcal{N}(0, \sigma_\chi^2(u_j)). \tag{31}$$

In addition, assuming that $\widehat{u}_j$ has support in $\mathbb{T}^2$, one has

$$\sigma_\chi^2(u_j) = \frac{(2\pi)^2}{c_X(u_j)^2}\left(1 + \frac{\sin(4\delta)}{4\delta} + \frac{3}{2}\left(\frac{\sin(2\delta)}{2\delta}\right)^2\right)\int_{\mathbb{R}^2} |\widehat{u}_j(\xi)|^4 f_{H,\delta}(\xi)^2 d\xi.$$

Proof. See Appendix. □

Figure 5 presents the results of the coherence index estimation from textures generated by lighthouse random fields with different parameters. Figure 5a) compares the empirical mean of estimations of the coherence index for 300 Monte-Carlo simulations at each scale, for $H = 0.5$ and various degrees of anisotropy. The target coherence index for each degree of anisotropy is displayed as a dotted line. We notice that depending on the degree of anisotropy, the first and last scales do not always allow a correct estimation of χ_X. We observe that for an image of initial size 1024×1024, the third scale appears to be the one providing the best results (see Section 5.2 for justifications). Figure 5b) presents the estimates obtained at scale $j = 3$ of the coherence index for various degrees of anisotropy (color) and various Hurst parameters (x-axis). The theoretical value is represented by a dotted line. When H is far from 0 or 1, the χ_X estimate is very accurate, regardless of the degree of anisotropy. In the elementary case, the coherence index is defined as the cardinal sine of the degree of anisotropy (multiplied by 2) and then a good estimate of the coherence index allows us to estimate δ the degree of anisotropy, by inverting the cardinal sine function, which is a bijection from $(0,\pi]$ to $[0,1)$.

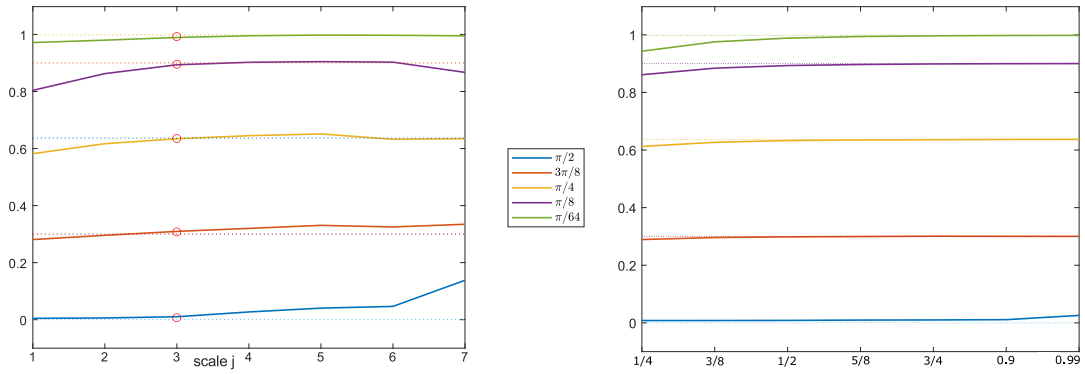

a) $H = 0.5$ b) $j = 3$

FIGURE 5. Empirical mean (solid lines) of $\chi_X(u_j)^{\text{emp}}$ given by (30), computed on 300 Monte-Carlo simulations with respect to a) the scale j and the degree of anisotropy $\delta \in \left\{\frac{\pi}{64}, \frac{\pi}{8}, \frac{\pi}{4}, \frac{3\pi}{8}, \frac{\pi}{2}\right\}$, for $H = 0.5$ and b) the degree of anisotropy $\delta \in \left\{\frac{\pi}{64}, \frac{\pi}{8}, \frac{\pi}{4}, \frac{3\pi}{8}, \frac{\pi}{2}\right\}$ and $H \in \left\{\frac{1}{4}, \frac{3}{8}, \frac{1}{2}, \frac{5}{8}, \frac{3}{4}, 0.9, 0.99\right\}$, using $j = 3$. The true values of the coherence index are given by the dotted lines.

6.3. **Estimation of the Hurst parameter.**

The eigenvalues of the structure tensor provide new estimators of the H index, as we have, for all scale $j \in \mathbb{Z}$,

$$\frac{\lambda^{\pm}(u_{j+1})}{\lambda^{\pm}(u_j)} = 2^{2H+2}. \tag{32}$$

Thus, we define two Hurst index estimators for a given scale j as

$$H_{\mathcal{R}j}^{+\text{emp}} = \frac{1}{2\log(2)} \log\left(\frac{\lambda_{j+1}^{+\text{emp}}}{\lambda_j^{+\text{emp}}}\right) - 1 \quad \text{and} \quad H_{\mathcal{R}j}^{-\text{emp}} = \frac{1}{2\log(2)} \log\left(\frac{\lambda_{j+1}^{-\text{emp}}}{\lambda_j^{-\text{emp}}}\right) - 1. \tag{33}$$

In the following, we then propose to estimate the Hurst index by averaging these two estimators, that is by

$$H_{\mathcal{R}j}^{\text{emp}} = \frac{H_{\mathcal{R}j}^{+\text{emp}} + H_{\mathcal{R}j}^{-\text{emp}}}{2}.$$

As for the previous estimators, we obtain the following proposition. Since the estimators $\lambda_j^{\pm\text{emp}}$ are strongly consistent estimators (see Proposition 6.4), by (32), $H_{\mathcal{R}j}^{\text{emp}}$ is also a strong consistent estimator of the Hurst index H.

Proposition 6.6. *Let $(H, \delta) \in (0,1) \times (0, \pi/2]$ and let X be the lighthouse field with spectral density $f_{H,\delta}$ given by (5). Let $u \in \mathcal{S}_0\left(\mathbb{R}^2\right)$ be a non-zero radial function and let $j \in \mathbb{Z}$. Then*

$$H_{\mathcal{R}j}^{emp} \xrightarrow[N\to\infty]{a.s.} H.$$

Remark 6.7. *Note that one may also prove that this estimator is also asymptotically normal. To do so, one can first establish the asymptotic normality of $\left(J_j^{emp}, J_{j+1}^{emp}\right)$, a vector of length 6 (still identifying the matrices J_j^{emp} and J_{j+1}^{emp} to vectors of length 3), by generalizing the proof done for the vector $\left(V_j^{emp}, V_{j+1}^{emp}\right) \in \mathbb{R}^2$ (see Proof of Theorem 5.4 in the Appendix) and then apply the Delta method.*

Figure 6a) displays the logarithm of the eigenvalues of the estimator J_j^{emp} computed at each scale j for a lighthouse field of parameters $H = 0.5$ and $\delta = \pi/4$. We choose to use $j = 3$ in our experiments as it seems to produce the best results. Figure 6a) illustrates the effect of the choice of scale: the estimate $H_{\mathcal{R}j}^{\text{emp}}$, computed using scales 3 and 4, gives the blues and red dotted lines whose slope coefficient is equal to $\log(2)(2H_{\mathcal{R}j}^{\text{emp}} + 2)$, while the black dotted line is given by the true Hurst index $H = 0.5$. Figure 6b) represents the various estimates of H obtained for lighthouse fields of different degrees of anisotropy and self-similarity orders. Similarly to the estimation of the coherence index, the quality of the estimation strongly depends on the value of H, regardless of the degree of anisotropy. This observation is consistent with theoretical results obtained in a similar framework studied by Biermé et al. [11]. On the other hand, when δ is close to 0, the estimation of H fails. Compared with Figure 4b), the monogenic approach improves significantly these results.

Table 2 presents the results of several estimation methods adapted to the isotropic case ($\delta = \pi/2$), and compare them with ours. The Soltani, Somar and Bochu (SSB) method [44] and the Tukey's trimean of the mid-energy (TTME) method [25] are also based on non-decimated wavelet transforms. Both estimators presented here significantly outperforms the other methods, regardless of the value of H. Comparing this table with Table 1, note that the estimator using the monogenic tensor produces performances of the same order as these standard methods only for extreme values of anisotropy ($\delta = \pi/64$) and Hurst index ($H = 0.99$). For all other anisotropy degrees and Hurst indexes, the mean squared error remains substantially lower.

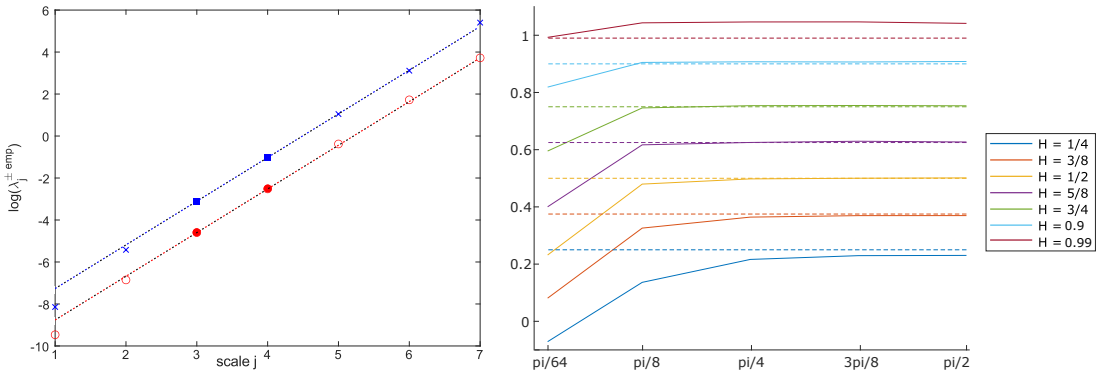

a) $\log\left(\lambda_j^{\pm \text{emp}}\right)$ for $H = 0.5$ and $\delta = \pi/4$ b) Empirical mean of $H_{\mathcal{R}3}^{\text{emp}}$

FIGURE 6. Estimation of H for an initial simulation of size 1024×1024 obtained by the eigenvalues $\lambda_j^{\pm \text{emp}}$ from $J_X(u_j)$ (a). Logarithm of the eigenvalues $\lambda_j^{\pm \text{emp}}$ with respect to the scale j, computed for one realization with $H = 0.5$ and $\delta = \pi/4$. Dotted lines are computed using two scales ($j = 3, 4$), with empirical slope in red for the smallest eigenvalue and in blue for the largest, and with theoretical slopes in black. (b). Empirical mean of $H_{\mathcal{R}3}^{\text{emp}}$ (solid lines) given by (33) computed on 300 Monte-Carlo simulations for $\delta \in \left\{\frac{\pi}{64}, \frac{\pi}{8}, \frac{\pi}{4}, \frac{3\pi}{8}, \frac{\pi}{2}\right\}$ and $H \in \left\{\frac{1}{4}, \frac{3}{8}, \frac{1}{2}, \frac{5}{8}, \frac{3}{4}, 0.9, 0.99\right\}$. The solid lines give the true values of H.

H	SSB [44]	TTME [25]	MonTens	StrucTens
MSE				
0.3	0.0016	0.0015	0.0002	0.0002
0.5	0.0019	0.0015	0.0001	0.0001
0.7	0.0025	0.0022	0.0001	0.0001
0.8	0.0027	0.0023	0.0001	0.0001
0.9	0.0032	0.0027	0.0002	0.0002
Variance				
0.3	0.0016	0.0015	0.0001	0.0001
0.5	0.0017	0.0013	0.0001	0.0001
0.7	0.0019	0.0018	0.0001	0.0001
0.8	0.0021	0.0018	0.0001	0.0001
0.9	0.0021	0.0018	0.0001	0.0001

TABLE 2. Comparison of the estimation procedures presented here for the isotropic case ($\delta = \pi/2$): Mean square error and empirical variance, computed on 300 Monte-Carlo simulations of size 1024×1024, for the estimation of the Hurst index H by the SSB method [44], the TTME method [25] and by the methods based on the monogenic tensor (MonTens) and on the structure tensor (StrucTens), respectively given by (23) and (33) using $j = 3$.

7. Rotation of a lighthouse field

In the previous sections, to simplify notations and computations, we have considered the specific case of lighthouse fields with a vertical anisotropy direction. That is because their spectral density were defined using a function t_δ based on a frequential cone on the unit sphere that is centered around the parameter $\Theta(0) = (1, 0) \in S^1$ (Equation (4)). Nevertheless, our results on the inference of these random fields parameters generalize to general lighthouse fields, presented in [14, 40].

Definition 7.1. *An anisotropic self-similar Gaussian random field Y is called a lighthouse field if its spectral density is defined by*

$$f_{H,\delta,\alpha_0}(\xi) = t_{\alpha_0,\delta}\left(\frac{\xi}{|\xi|}\right)|\xi|^{-2H-2}, \tag{34}$$

with $\alpha_0 \in [\frac{-\pi}{2}, \frac{\pi}{2})$, $H \in (0,1)$ the Hurst parameter, $\delta \in \left(0, \frac{\pi}{2}\right]$ and $t_{\alpha_0,\delta} : S^1 \to [0, \infty)$ the even function such that

$$\forall\, \alpha \in \left[\alpha_0 - \frac{\pi}{2}, \alpha_0 + \frac{\pi}{2}\right], \quad t_{\alpha_0,\delta}\left(\Theta(\alpha)\right) = \mathbf{1}_{[\alpha_0-\delta,\, \alpha_0+\delta]}(\alpha)$$

where we recall that

$$\Theta(\alpha) = (\cos(\alpha), \sin(\alpha)) \in S^1.$$

In this definition, as before, δ is half the width of the frequential cone. It defines the degree of anisotropy in the associated texture. The new parameter α_0 changes the orientation of the frequential cone defined by f_{H,δ,α_0}, it gives the orthogonal orientation of the anisotropic random field. For $\alpha \in \mathbb{T}$, we introduce

$$R_\alpha = \begin{pmatrix} \cos(\alpha) & -\sin(\alpha) \\ \sin(\alpha) & \cos(\alpha) \end{pmatrix},$$

the 2 dimensional rotation matrix of angle α and recall that $R_\alpha^* = R_{-\alpha}$. Noting that

$$f_{H,\delta,\alpha_0}(\xi) = f_{H,\delta}(R_{\alpha_0}^* \xi),$$

it follows that the spectral density of the monogenic field $\mathcal{M}Y(u)$, defined for some radial $u \in \mathcal{S}_0(\mathbb{R})$ is given by

$$f_{\mathcal{M}Y}(\xi) = C_{\mathcal{M}}(\xi) f_{\alpha_0}(\xi) = S_{\alpha_0} f_{\mathcal{M}X}(R_{\alpha_0}^* \xi) S_{\alpha_0}^*, \tag{35}$$

where $f_{\mathcal{M}X}$ is given by (13), using the fact that

$$C_{\mathcal{M}}(\xi) = S_{\alpha_0} C_{\mathcal{M}}(R_{\alpha_0}^* \xi) S_{\alpha_0}^*,$$

with

$$S_{\alpha_0} = \begin{pmatrix} 1 & 0 \\ 0 & R_{\alpha_0} \end{pmatrix}$$

the 3 dimensional rotation matrix of angle α_0 and axis $(1,0,0)$. Hence the stationary vectorial random field $(\mathcal{M}Y(\tau_x u))_{x\in\mathbb{R}^2}$ satisfies

$$(\mathcal{M}Y(\tau_x u))_{x\in\mathbb{R}^2} \overset{fdd}{=} \left(S_{\alpha_0} \mathcal{M}X(\tau_{R_{\alpha_0}^* x} u)\right)_{x\in\mathbb{R}^2}.$$

Then Proposition 3.6 and Theorem 3.7 rewrite as the following proposition.

Theorem 7.2. *Let $(H,\delta) \in (0,1)\times(0,\pi/2]$. Let $\alpha_0 \in (-\pi/2, \pi/2]$ and Y be the lighthouse field with spectral density f_{H,δ,α_0} defined by (34). Let $u \in \mathcal{S}_0(\mathbb{R}^2)$ be a radial function. Then $(\mathcal{M}Y(\tau_x u))_{x\in\mathbb{R}^2}$ is a centered stationary vectorial Gaussian field with spectral density given by*

$$f_{\mathcal{M}Y,u}(\xi) = f_{\mathcal{M}Y}(\xi)|\widehat{u}(\xi)|^2 = S_{\alpha_0} f_{\mathcal{M}X}((R_{\alpha_0}^*\xi) S_{\alpha_0}^* \text{ for a.e. } \xi \in \mathbb{R}^2, \tag{36}$$

where $f_{\mathcal{M}Y}$ is defined in (35). Therefore,

$$\mathcal{M}Y(\tau_x u) \overset{d}{=} S_{\alpha_0} \mathcal{M}X(\tau_{R_{\alpha_0}^* x} u) \overset{d}{=} S_{\alpha_0} \sqrt{c_X(u)} D_\delta Z,$$

with

$$c_X(u) = \mathrm{Var}(\langle X, u\rangle) = \int_{\mathbb{R}^2} |\widehat{u}(\xi)|^2 f_{H,\delta}(\xi) d\xi = \mathrm{Var}(\langle Y, u\rangle),$$

the diagonal matrix

$$D_\delta = \mathrm{diag}\left(1, \sqrt{\frac{1}{2} + \frac{\sin(2\delta)}{4\delta}}, \sqrt{\frac{1}{2} - \frac{\sin(2\delta)}{4\delta}}\right)$$

and $Z \sim \mathcal{N}(0, I_3)$. Moreover, for a given scale j,

$$(\mathcal{M}Y(\tau_x u_j))_{x\in\mathbb{R}^2} \overset{d}{=} 2^{j(H+1)} (\mathcal{M}Y(\tau_{2^{-j}x} u))_{x\in\mathbb{R}^2}.$$

Finally the spherical coordinates satisfy

$$(A_Y(\tau_x u), \varphi_Y(\tau_x u), \theta_Y(\tau_x u))_{x\in\mathbb{R}^2} \overset{fdd}{=} \left(A_X(\tau_{R_{\alpha_0}^* x} u), \varphi_X(\tau_{R_{\alpha_0}^* x} u), \theta_X(\tau_{R_{\alpha_0}^* x} u) + \alpha_0\right)_{x\in\mathbb{R}^2}.$$

Hence $\theta_Y(u)$ follows an offset normal distribution whose probability density function is given by

$$t \mapsto \frac{\sqrt{1-\chi_Y(u)^2}}{2\pi(1-\chi_Y(u)\cos(2(t-\alpha_0))},$$

where $\chi_Y(u) = \chi_X(u) \in [0,1)$ is the coherence index given by (18).

Figure 7 presents the empirical probability density functions of the amplitude, the phase and the orientation of the monogenic signal computed on one realization of three different lighthouse fields of parameters $H = 0.5$, $\delta = \pi/6$ and a rotation offset $\alpha_0 = 0$, $\alpha_0 = -\pi/8$ and $\alpha_0 = \pi/4$. This figure illustrates how the orientation of the field α_0 only impacts the monogenic signal's orientation, by translating its probability density function of α_0.

As we now assume to observe $\mathcal{M}Y(\tau_x u_j)$ for $x \in \mathcal{G}_N$, for some radial function u and at different scales j, we can proceed as previously by considering $\mathcal{T}M_j^{\mathrm{emp}}$ as in (19) where X is replaced by Y. It follows that a consistent and asymptotically normal estimator of the mean square amplitude $\mathbb{E}(A_Y(u_j)^2)$ $\left(= \mathbb{E}(A_X(u_j)^2)\right)$ is still obtained by considering $\mathrm{Tr}\left(\mathcal{T}M_j^{\mathrm{emp}}\right)$ and therefore we can use the same procedure detailed in Section 5.2 to estimate the Hurst index. However, the Riesz structure tensor (see Definition 6.1) becomes

$$J_Y(u_j) = R_{\alpha_0} J_X(u_j) R_{\alpha_0}^* = R_{\alpha_0} \mathrm{diag}\left(\lambda^+(u_j), \lambda^-(u_j)\right) R_{\alpha_0}^*.$$

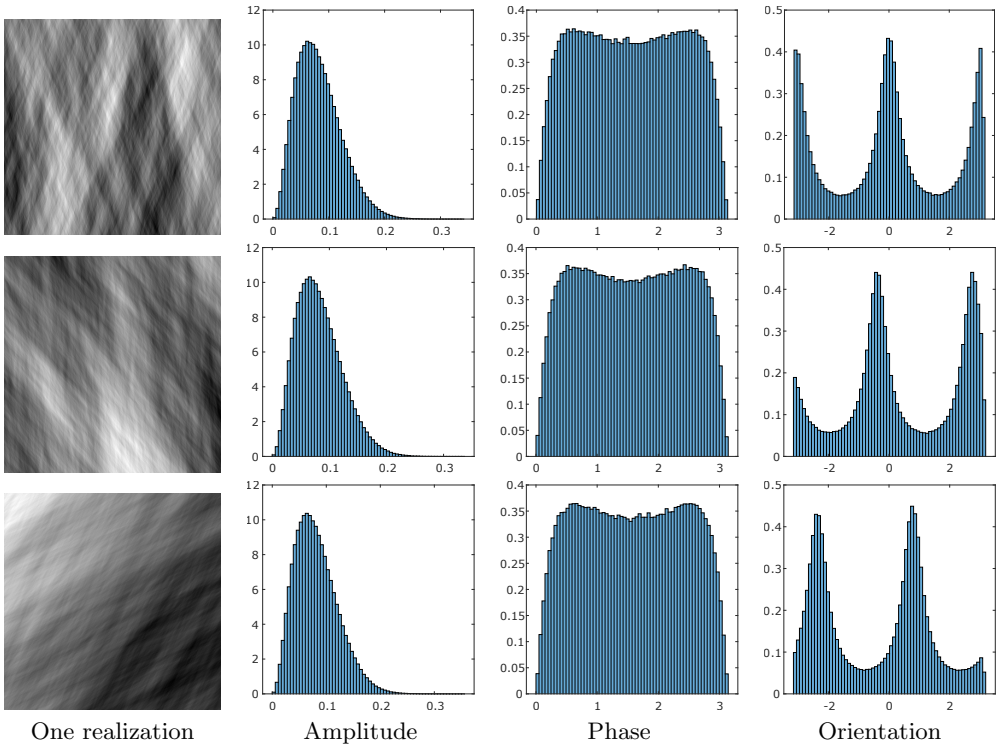

FIGURE 7. Empirical probability density functions of the amplitude, phase and orientation of the monogenic signal of a lighthouse fields with parameters $H = 0.5$, $\delta = \pi/6$ and a rotation offset $\alpha_0 = 0$ (top), $\alpha_0 = -\pi/8$ (middle), $\alpha_0 = \pi/4$ (bottom), computed on one realization of size 1024×1024.

Therefore $J_Y(u_j)$ has the same eigenvalues as $J_X(u_j)$ but its eigenvectors are rotated from those of $J_X(u_j)$. Hence, considering $J_j^{\text{emp}} = \left[\mathcal{T} M_j^{\text{emp}}\right]_{2\leq,q\leq 3}$ as in (25), Proposition 6.2 may be generalized to get a consistent and asymptotically normal estimator of $J_Y(u_j)$ and of the coherence index by considering $\lambda_j^{+\text{emp}}$ the largest eigenvalue of J_j^{emp} and $\lambda_j^{-\text{emp}}$ the smallest one. When $\lambda^+(u_j) > \lambda^-(u_j)$, (or equivalently $\delta \in (0, \frac{\pi}{2})$), then, we may define $\alpha_{0,j}^{\text{emp}} \in (-\pi/2, \pi/2)$ be such that $\Theta(\alpha_{0,j}^{\text{emp}})$ is a unit eigenvector of J_j^{emp} with respect to the greatest eigenvalue $\lambda_j^{+\text{emp}}$. Note that when $\lambda_j^{+\text{emp}} = \lambda_j^{-\text{emp}}$, we simply set $\alpha_{0,j}^{\text{emp}} = 0$. We present in Figure 8, the results of this procedure. Empirical mean of $\alpha_{0,3}^{\text{emp}}$ over 150 Monte-Carlo simulations are computed for different values of $H \in \{1/4, 3/8, 1/2, 5/8, 3/4, 0.9, 0.99\}$, and rotation $\alpha_0 \in \{-\pi/4, -\pi/8, 0, \pi/8, \pi/4, \pi/3\}$ in three different anisotropic cases $\delta \in \{3\pi/8, \pi/8, \pi/4\}$. Recall that this procedure has no sense for δ close to $\pi/2$ since the field is isotropic. Moreover, the closer to 0 the angle δ is, the better the orientation of the rotation is estimated.

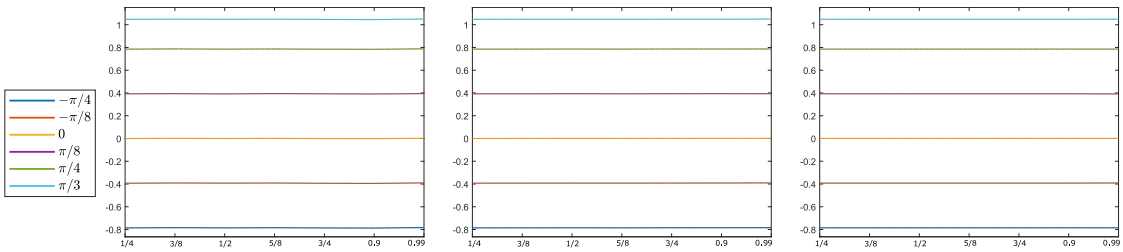

FIGURE 8. Empirical mean of $\alpha_{0,3}^{\text{emp}}$ (solid lines), computed on 150 Monte-Carlo simulations for $H \in \left\{\frac{1}{4}, \frac{3}{8}, \frac{1}{2}, \frac{5}{8}, \frac{3}{4}, 0.9, 0.99\right\}$, $\alpha_0 \in \{-\pi/4, -\pi/8, 0, \pi/8, \pi/4, \pi/3\}$ and (a) $\delta = 3\pi/8$, (b) $\delta = \pi/8$ and (c) $\delta = \pi/64$.

8. Conclusion

This paper described a new strategy to analyse a lighthouse anisotropic fractional Brownian fields (AFBFs), characterized by different parameters: the Hurst index for scale invariance and the coherence index for degree of anisotropy, that give the structural information of the texture. Estimating the model parameters is a crucial issue for modeling and analyzing real data. It is therefore essential to propose an estimation strategy that is theoretically validated with respect to the properties of these estimators, while also relying on a robust numerical methodology. In this paper, we have proposed a new methodology using the monogenic transform, which provides a comprehensive representation of the analyzed texture in a multi-scale context.

The multi-scale monogenic representation of lighthouse fields, introduced in this paper, enabled us to define strongly consistent estimators of both the coherence and Hurst index, that parameterize these fields. We have shown that the monogenic signal of a lighthouse field is a stationary Gaussian random field. Thanks to the properties of the monogenic signal, we have demonstrated that these estimators adhere to theoretical guarantees of convergence, in particular, asymptotic normality.

We discussed a numerical scheme for computing the monogenic transform that adheres to the necessary constraints in order to preserve the theoretically established qualities of the estimators. Different implementation choices have been proposed and discussed, both regarding the computation of the representation and the practical application of the estimators. Our numerical simulations show that these estimators are robust to various values of parameters and outperform standard estimation methods in the isotropic case. Our methodology is also robust for rotation of texture and allows to estimate the induced direction of anisotropy.

Appendix A. Proofs

Proof of Proposition 3.4.

(i) Let $u, v \in \mathcal{S}_0(\mathbb{R}^2)$ be two real-valued function. Then the covariance between the two vectors $\mathcal{M}X(u)$ and $\mathcal{M}X(v)$ is

$$\begin{aligned}\mathcal{C}_{\mathcal{M}X}(u,v) &= \mathbb{E}\left(\mathcal{M}X(u)\mathcal{M}X(v)^*\right)\\ &= \mathbb{E}\begin{pmatrix} \langle X,u\rangle\langle X,v\rangle & -\langle X,u\rangle\langle X,\mathcal{R}_1 v\rangle & -\langle X,u\rangle\langle X,\mathcal{R}_2 v\rangle \\ -\langle X,\mathcal{R}_1 u\rangle\langle X,v\rangle & \langle X,\mathcal{R}_1 u\rangle\langle X,\mathcal{R}_1 v\rangle & \langle X,\mathcal{R}_1 u\rangle\langle X,\mathcal{R}_2 v\rangle \\ -\langle X,\mathcal{R}_2 u\rangle\langle X,v\rangle & \langle X,\mathcal{R}_2 u\rangle\langle X,\mathcal{R}_1 v\rangle & \langle X,\mathcal{R}_2 u\rangle\langle X,\mathcal{R}_2 v\rangle \end{pmatrix}\end{aligned}$$

by definition of $\mathcal{R}_k X$. Hence, by (7) and by (9), we have:

$$\mathcal{C}_{\mathcal{M}X}(u,v) = \int_{\mathbb{R}^2} \widehat{u}(\xi)\overline{\widehat{v}(\xi)} f_{\mathcal{M}X}(\xi) d\xi$$

with

$$f_{\mathcal{M}X}(\xi) = \begin{pmatrix} 1 & -i\frac{\xi_1}{|\xi|} & -i\frac{\xi_2}{|\xi|} \\ i\frac{\xi_1}{|\xi|} & \frac{\xi_1^2}{|\xi|^2} & \frac{\xi_1\xi_2}{|\xi|^2} \\ i\frac{\xi_2}{|\xi|} & \frac{\xi_1\xi_2}{|\xi|^2} & \frac{\xi_2^2}{|\xi|^2} \end{pmatrix} f(\xi).$$

(ii) By Equation (12), for $k = 1, 2$

$$\mathrm{Cov}\left(\langle X,u\rangle, \langle \mathcal{R}_k X,u\rangle\right) = -\Re\int_{\mathbb{R}^2} \frac{i\xi_k}{|\xi|} |\widehat{u}(\xi)|^2 f(\xi)\, d\xi = -\int_{\mathbb{R}^2} \frac{i\xi_k}{|\xi|} |\widehat{u}(\xi)|^2 f(\xi)\, d\xi = 0$$

since $|\widehat{u}|^2 f$ is a real-valued function. Hence since $\mathcal{M}X(u)$ is a centered Gaussian random vector with values in $\mathbb{R}^3$, $\langle X,u\rangle$ and $\mathcal{R}X(u)$ are independent.

(iii) As the generalized field $\mathcal{M}X$, $(\mathcal{M}X(\tau_x u))_{x\in\mathbb{R}^2}$ is a centered Gaussian random field. Moreover, by (12), its covariance function is given by

$$\mathcal{C}_{\mathcal{M}X}(\tau_x u, \tau_y u) = \int_{\mathbb{R}^2} e^{-i(x-y)\cdot\xi} |\widehat{u}(\xi)|^2 f_{\mathcal{M}X}(\xi) d\xi = \mathcal{C}_{\mathcal{M}X}(\tau_{x-y}u, u)$$

and so the random field $(\mathcal{M}X(\tau_x u))_{x\in\mathbb{R}^2}$ is stationary and, its spectral density is given by (14).

(iv) Let us now assume that the spectral density f is defined by (3). Then, for a given scale j, since $\widehat{u}_j(\xi) = 2^j\widehat{u}(2^j\xi)$, by a change of variable we get

$$\begin{aligned}\mathcal{C}_{\mathcal{M}X}(\tau_x u_j, \tau_y u_j) &= \int_{\mathbb{R}^2} e^{-i(x-y)\cdot\xi} 2^{2j} |\widehat{u}(2^j\xi)|^2 f_{\mathcal{M}X}(\xi) d\xi\\ &= \int_{\mathbb{R}^2} e^{-i(x-y)\cdot 2^{-j}\xi} |\widehat{u}(\xi)|^2 f_{\mathcal{M}X}(2^{-j}\xi) d\xi.\end{aligned}$$

Hence by Equation (3), we have

$$\begin{aligned}\mathcal{C}_{\mathcal{M}X}\left(\tau_x u_j, \tau_y u_j\right) &= 2^{j(2H+2)} \int_{\mathbb{R}^2} e^{-i(x-y)\cdot 2^{-j}\xi} |\widehat{u}(\xi)|^2 f_{\mathcal{M}X}(\xi) d\xi \\ &= 2^{j(2H+2)} \mathcal{C}_{\mathcal{M}X}\left(\tau_{2^{-j}x} u, \tau_{2^{-j}y} u\right),\end{aligned}$$

which concludes the proof since $(\mathcal{M}X(\tau_x u_j))_{x\in\mathbb{R}^2}$ and $(\mathcal{M}X(\tau_{2^{-j}x} u))_{x\in\mathbb{R}^2}$ are two Gaussian centered random fields.

□

Proof of Proposition 3.6. By definition, the vector $\mathcal{M}X(u)$ is a centered Gaussian vector and so we only have to compute its covariance matrix

$$\mathcal{C}_{\mathcal{M}X}(u,u) = \int_{\mathbb{R}^2} |\widehat{u}(\xi)|^2 f_{\mathcal{M}X}(\xi) d\xi.$$

By Proposition 3.4, we first have

$$\mathrm{Cov}\left(\langle X, u\rangle, \langle \mathcal{R}_k X, u\rangle\right) = 0.$$

Moreover, setting $\mathrm{e}_1 = (1,0) \in S^1$ and applying a change of variable in polar coordinates, since u is radial, we have

$$\mathrm{Cov}\left(\langle \mathcal{R}_1 X, u\rangle, \langle \mathcal{R}_2 X, u\rangle\right) = 2\int_0^{+\infty} \int_{-\pi/2}^{\pi/2} \frac{\sin(2\alpha)}{2} |\widehat{u}(r\mathrm{e}_1)|^2 r^{-2H-1} \mathbf{1}_{|\alpha|\le\delta}\, d\alpha dr = 0.$$

Similarly we have

$$\begin{aligned}\mathrm{Var}\left(\langle \mathcal{R}_1 X, u\rangle\right) &= 2\int_0^{+\infty} \int_{-\pi/2}^{\pi/2} \cos^2(\alpha) |\widehat{u}(r\mathrm{e}_1)|^2 r^{-2H-1} \mathbf{1}_{|\alpha|\le\delta}\, d\alpha dr \\ &= (2\delta + \sin(2\delta)) \int_0^{+\infty} |\widehat{u}(r\mathrm{e}_1)|^2 r^{-2H-1} dr\end{aligned}$$

and

$$\begin{aligned}\mathrm{Var}\left(\langle \mathcal{R}_2 X, u\rangle\right) &= 2\int_0^{+\infty} \int_{-\pi/2}^{\pi/2} \sin^2(\alpha) |\widehat{u}(r\mathrm{e}_1)|^2 r^{-2H-1} \mathbf{1}_{|\alpha|\le\delta} d\alpha dr \\ &= (2\delta - \sin(2\delta)) \int_0^{+\infty} |\widehat{u}(r\mathrm{e}_1)|^2 r^{-2H-1} dr.\end{aligned}$$

The proof is then concluded noting that we also have

$$\mathrm{Var}(\langle X, u\rangle) = 2\int_0^{+\infty} \int_{-\pi/2}^{\pi/2} |\widehat{u}(r\mathrm{e}_1)|^2 r^{-2H-1} \mathbf{1}_{|\alpha|\le\delta} d\alpha dr = 4\delta \int_0^{+\infty} |\widehat{u}(r\mathrm{e}_1)|^2 r^{-2H-1} dr.$$

□

Proof of Theorem 3.7.

(i) The first assertion is a direct consequence of the stationarity of the random field $(\mathcal{M}X(\tau_x u))_{x\in\mathbb{R}^2}$ stated in Proposition 3.4.

(ii) By Proposition 3.6, the Riesz vector $\mathcal{R}X(u) = (\langle \mathcal{R}_1 X, u\rangle, \langle \mathcal{R}_2 X, u\rangle)$ is a centered Gaussian random vector with covariance matrix

$$c_X(u)\mathrm{diag}\left(\frac{1}{2} + \frac{\sin(2\delta)}{4\delta}, \frac{1}{2} - \frac{\sin(2\delta)}{4\delta}\right).$$

Note that since u is a non zero function, $c_X(u) \neq 0$ and then this covariance matrix is positive. Moreover, the polar coordinates $\mathcal{R}X(u)$ are $(A_X(u)\sin\varphi_X(u), \theta_X(u)) \in [0,+\infty) \times [-\pi,\pi)$. Then, from [28] (see page 43), the density function of the angle $\theta_X(u)$ is given by

$$\theta \mapsto \frac{\sqrt{1-b^2}}{2\pi(1 - b\cos(2\theta))},$$

with

$$b = \frac{\mathrm{Var}\left(\langle \mathcal{R}_1 X, u\rangle\right) - \mathrm{Var}\left(\langle \mathcal{R}_2 X, u\rangle\right)}{\mathrm{Var}\left(\langle \mathcal{R}_1 X, u\rangle\right) + \mathrm{Var}\left(\langle \mathcal{R}_2 X, u\rangle\right)} = \frac{\sin(2\delta)}{2\delta} := \chi_X(u).$$

(iii) By Proposition 3.6,

$$A_X(u)^2 = |\mathcal{M}X(u)|^2 \overset{d}{=} c_X(u) A_\delta^2$$

with $A_\delta = D_\delta Z$ and Z a standard Gaussian vector. Since A_δ^2 is the squared norm of a Gaussian random vector, its distribution is a Generalized chi-square one. Moreover,

$$\mathbb{E}\left(A_\delta^2\right) = \mathrm{Tr}\left(D_\delta^2\right) = 2.$$

(iv) Let us now assume that $\delta = \pi/2$. First, $\chi_X(u) = 0$ and so $\theta_X(u)$ follows the uniform distribution on $(-\pi, \pi)$. Moreover, by Proposition 3.6, $\mathcal{M}X(u)$ is a centered Gaussian random vector with covariance matrix

$$c_X(u) \begin{pmatrix} 1 & 0 & 0 \\ 0 & 1/2 & 0 \\ 0 & 0 & 1/2 \end{pmatrix}.$$

Therefore, its density is the function

$$(t_1, t_2, t_3) \mapsto \frac{1}{\pi\sqrt{2\pi c_X(u)^3}} e^{-\frac{t_1^2}{2c_X(u)}} e^{-\frac{t_2^2+t_3^2}{c_X(u)}}.$$

Applying a change of variables into spherical coordinates, we obtain that the joint density of $(A_X(u), \varphi_X(u), \theta_X(u))$ is

$$(a, \phi, \theta) \mapsto \frac{1}{\pi\sqrt{2\pi c_X(u)^3}} e^{-\frac{a^2\cos^2(\phi)}{2c_X(u)}} e^{-\frac{a^2\sin^2(\phi)}{c_X(u)}} r^2 \sin(\phi)\, \mathbb{1}_{(0,+\infty)}(a) \mathbb{1}_{(0,\pi)}(\phi)\, \mathbb{1}_{(-\pi,\pi)}(\theta).$$

Hence $\theta_X(u)$ is independent from $(A_X(u), \varphi_X(u))$. Moreover, the joint density of $(A_X(u), \varphi_X(u))$ is

$$(a, \phi) \mapsto \sqrt{\frac{2}{\pi c_X(u)^3}}\, e^{-\frac{a^2(1+\sin^2(\phi))}{2c_X(u)}} a^2 \sin(\phi) \mathbf{1}_{(0,+\infty)}(a) \mathbf{1}_{(0,\pi)}(\phi).$$

By integrating with respect to a, $\varphi_X(u)$ admits the expected density function.

(v) Let now $j \in \mathbb{Z}$. Then by Proposition 3.4,

$$\mathcal{M}X(u_j) \overset{d}{=} 2^{j(H+1)} \mathcal{M}X(u).$$

Therefore, in terms of spherical coordinates, see (16), we have

$$\begin{cases} A_X(u_j) & \overset{d}{=} & 2^{j(H+1)} A_X(u) \\ \vec{v}_X(u_j) & \overset{d}{=} & \vec{v}_X(u). \end{cases}$$

□

Proof of Theorem 5.2. As we identify a symmetric matrix of $\mathcal{M}_3(\mathbb{R})$ with a vector of $\mathbb{R}^6$, we first define the function $G : \mathbb{R}^3 \mapsto \mathbb{R}^6$ as

$$G(y_1, y_2, y_3) = (y_1^2, y_2^2, y_3^2, y_1y_2, y_1y_3, y_2y_3) \tag{37}$$

for $y = (y_1, y_2, y_3) \in \mathbb{R}^3$. Then, the result will follow once proven the following strong law of large numbers for

$$\mathcal{T}M_j^{\text{emp}} = \frac{1}{N^2} \sum_{x \in \mathcal{G}_N} G\left(\mathcal{M}X(\tau_x u_j)\right) \longrightarrow \mathbb{E}\left(G\left(\mathcal{M}X(u_j)\right)\right) \text{ a.s.}$$

and the vectorial central limit theorem

$$\frac{1}{N}\left(\sum_{x \in \mathcal{G}_N} \left[G\left(\mathcal{M}X(\tau_x u_j)\right) - \mathbb{E}\left(G\left(\mathcal{M}X(u_j)\right)\right)\right]\right) \longrightarrow \mathcal{N}\left(0, \Gamma_{\mathcal{T}M}(u_j)\right), \tag{38}$$

with $\Gamma_{\mathcal{T}M}(u_j) \in \mathcal{M}_6(\mathbb{R})$ an asymptotic covariance matrix detailed in the sequel. To prove this we will use Theorem 4 in [4] and its natural vectorial extension. According to Proposition 3.6, $(\mathcal{M}X(\tau_x u_j))_{x \in \mathbb{R}^2}$ is a stationary centered field, therefore $\mathbb{E}(\mathcal{T}M_j^{\text{emp}}) = \mathcal{T}_{MX}(u_j)$ and we can define for $x \in \mathbb{R}^2$,

$$r_j^{(p,q)}(x) = \text{Cov}\left([\mathcal{M}X(u_j)]_p, [\mathcal{M}X(\tau_x u_j)]_q\right) = \mathbb{E}\left([\mathcal{M}X(u_j)]_p [\mathcal{M}X(\tau_x u_j)]_q\right), \tag{39}$$

for $1 \le p, q \le 3$. Following Theorem 3.2 of [11], recalling (13), we may write for $x \in \mathbb{R}^2$

$$r_j^{(p,q)}(x) = \mathcal{C}_{\mathcal{M}X}^{(p,q)}(u_j, \tau_x u_j) = \int_{\mathbb{R}^2} e^{ix\cdot\xi} C_{\mathcal{M}}^{(p,q)}(\xi) |\widehat{u}_j(\xi)|^2 f_{H,\delta}(\xi) d\xi$$

where $\mathcal{C}_{\mathcal{M}X}^{(p,q)}(\cdot,\cdot)$ (respectively $C_{\mathcal{M}}^{(p,q)}(\cdot,\cdot)$) is the (p,q) entry of the matrix $\mathcal{C}_{\mathcal{M}X}^{(p,q)}(\cdot,\cdot)$ (respectively $C_{\mathcal{M}}(\cdot,\cdot)$). Then we have

$$r_j^{(p,q)}(x) = \int_{\mathbb{T}^2} e^{ix\cdot\xi} \overline{f}_j^{(p,q)}(\xi) d\xi, \tag{40}$$

where $\mathbb{T}^2 = [-\pi, \pi)^2$ and for a.e $\xi \in \mathbb{T}^2$

$$\overline{f}_j^{(p,q)}(\xi) = C_{\mathcal{M}}^{(p,q)}(\xi) |\widehat{u}_j(\xi)|^2 f_{H,\delta}(\xi) + R_j^{(p,q)}(\xi), \tag{41}$$

with

$$R_j^{(p,q)}(\xi) = \sum_{k \in \mathbb{Z}^2 \setminus \{0\}} C_{\mathcal{M}}^{(p,q)}(\xi + 2k\pi) |\widehat{u}_j(\xi + 2k\pi)|^2 f_{H,\delta}(\xi + 2k\pi).$$

Since $R_j^{(p,q)} \in L^\infty(\mathbb{T}^2) \subset L^2(\mathbb{T}^2)$ we obtain that $\overline{f}_j^{(p,q)} \in L^2(\mathbb{T}^2)$ as soon as

$$\int_{\mathbb{T}^2} |\widehat{u}_j(\xi)|^4 f_{H,\delta}(\xi)^2 d\xi < +\infty,$$

which is satisfied when $H < 1/2$ or choosing $u \in \mathcal{S}_1(\mathbb{R}^2)$ when $1/2 \leq H < 1$. In this case we obtain by Parseval's identity

$$\sum_{x\in\mathbb{Z}^2} |r_j^{(p,q)}(x)|^2 = (2\pi)^2 \int_{\mathbb{T}^2} |\overline{f}_j{}^{(p,q)}(\xi)|^2 d\xi < +\infty.$$

Then it is sufficient to check that writing $G = (G_l)_{1\leq l\leq 6}$, each coordinates G_l has Hermite rank greater than 2 (see Equation (2.2) in [4]). That follows from the fact that for all $l \in \{1,\dots,6\}$ and $p \in \{1,2,3\}$ one has

$$\mathbb{E}\left((G_l\left(\mathcal{M}X\left(u_j\right)\right) - \mathbb{E}\left(G_l\left(\mathcal{M}X\left(u_j\right)\right)\right)\right)[\mathcal{M}X(u_j)]_p) = 0,$$

using the fact that for all $p, p' \in \{1,2,3\}$ with $p' \neq p$,

$$\begin{cases} \mathbb{E}\left([\mathcal{M}X(u_j)]_p\right) = \mathbb{E}\left([\mathcal{M}X(u_j)]_p^3\right) = 0 \\ \mathbb{E}\left([\mathcal{M}X(u_j)]_p^2[\mathcal{M}X(u_j)]_{p'}\right) = \mathbb{E}\left([\mathcal{M}X(u_j)]_p^2\right)\mathbb{E}\left([\mathcal{M}X(u_j)]_{p'}\right) = 0 \\ \mathbb{E}\left([\mathcal{M}X(u_j)]_1[\mathcal{M}X(u_j)]_2[\mathcal{M}X(u_j)]_3\right) = 0 \end{cases}$$

since, by Proposition 3.6 the variables $[\mathcal{M}X(u_j)]_p$ and $[\mathcal{M}X(u_j)]_{p'}$ are independent symmetric random variables. Then by the vectorial extension of Theorem 4 in [4] (using for instance Cramer-Wold device), we obtain the central limit theorem with for any $1 \leq l, l' \leq 6$

$$[\Gamma_{\mathcal{T}M}(u_j)]_{l,l'} = \sum_{x\in\mathbb{Z}^2} \mathrm{Cov}(G_l(\mathcal{M}X(u_j)), G_{l'}(\mathcal{M}X(\tau_x u_j)), \tag{42}$$

and in particular, for $p, q \in \{1,2,3\}$,

$$[\Gamma_{\mathcal{T}M}(u_j)]_{p,q} = \sum_{x\in\mathbb{Z}^2} \mathrm{Cov}\left([\mathcal{M}X(u_j)]_p^2, [\mathcal{M}X(\tau_x u_j)]_q^2\right).$$

Since $\mathcal{M}X$ is a centered Gaussian random vector and since $\mathrm{Cov}(Z_1^2, Z_2^2) = 2\mathrm{Cov}(Z_1, Z_2)^2$ when (Z_1, Z_2) is a centered Gaussian vector, we then have

$$[\Gamma_{\mathcal{T}M}(u_j)]_{p,q} = 2\sum_{x\in\mathbb{Z}^2} |r_j^{(p,q)}(x)|^2 = 8\pi^2 \int_{\mathbb{T}^2} |\overline{f}_j{}^{(p,q)}(\xi)|^2 d\xi \tag{43}$$

for $p, q \in \{1,2,3\}$. Moreover, for $p \in \{1,2,3\}$ and $\xi \neq 0$, $C_{\mathcal{M}}^{(p,p)}(\xi) > 0$ and then $\overline{f}_j{}^{(p,p)}$ is a non zero and non negative function since u is a non zero function. Hence, $[\Gamma_{\mathcal{T}M}(u_j)]_{p,p} > 0$ for any $p \in \{1,2,3\}$ and $\Gamma_{\mathcal{T}M}(u_j) \neq 0$. In addition, again by the vectorial extension of Theorem 4 in [4], one can find $c > 0$ such that

$$\begin{aligned} \mathbb{E}\left(N^2\left[\frac{1}{N^2}\sum_{x\in\mathcal{G}_N}\left[G_l\left(\mathcal{M}X(\tau_x u_j)\right) - \mathbb{E}\left(G_l\left(\mathcal{M}X(u_j)\right)\right)\right]\right]^2\right) \\ \leq c\mathbb{E}\left(\left[G_l\left(\mathcal{M}X(u_j)\right) - \mathbb{E}\left(G_l\left(\mathcal{M}X(u_j)\right)\right)\right]^2\right). \end{aligned}$$

Hence by Theorem 3.2.1 of [26] we also have the almost sure convergence. □

Proof of Corollary 5.3. The strong consistency and the asymptotic normality with

$$\sigma^2(u_j) = \sum_{p,q=1}^{3} [\Gamma_{\mathcal{T}M}(u_j)]_{p,q}$$

follows immediately from Theorem 5.2. Note that $\sigma^2(u_j) > 0$ since $[\Gamma_{\mathcal{T}M}(u_j)]_{p,p} > 0$ for $p \in \{1,2,3\}$ according to the proof of Theorem 5.2. Moreover, by (43),

$$\sigma^2\left(u_j\right) = 8\pi^2 \sum_{p,q=1}^{3} \int_{\mathbb{T}^2} |\overline{f}_j{}^{(p,q)}(\xi)|^2 d\xi,$$

with $\overline{f}_j{}^{(p,q)}$ defined by (41). Then, if $\widehat{u}_j$ has support in $\mathbb{T}^2$, by (41),

$$\sigma^2\left(u_j\right) = 8\pi^2 \int_{\mathbb{T}^2} \sum_{p,q=1}^{3} |C_{\mathcal{M}}^{(p,q)}(\xi)|^2 |\widehat{u}_j(\xi)|^4 f_{H,\delta}(\xi)^2 d\xi = 32\pi^2 \int_{\mathbb{T}^2} |\widehat{u}_j(\xi)|^4 f_{H,\delta}(\xi)^2 d\xi,$$

since $\sum_{p,q=1}^{3} |C_{\mathcal{M}}^{(p,q)}(\xi)|^2 = 4$ for all $\xi \neq 0$, which concludes the proof. □

Proof of Theorem 5.4. First the strong consistency follows from (22) and Corollary 5.3. We then have to prove that the couple $\left(V_j^{\rm emp}, V_{j+1}^{\rm emp}\right)$ satisfies asymptotic normality. By [38] since we already have the asymptotic normality of each marginals (see Corollary 5.3), it suffices to check that there exists $\rho(u_j)$ such that

$$N^2 {\rm Cov}\left(V_j^{\rm emp}, V_{j+1}^{\rm emp}\right) \xrightarrow[N\to\infty]{} \rho(u_j).$$

But now, using again the fact that ${\rm Cov}(Z_1^2, Z_2^2) = 2{\rm Cov}(Z_1, Z_2)^2$ when (Z_1, Z_2) is a centered Gaussian vector,

$$\begin{aligned} N^2 {\rm Cov}\left(V_j^{\rm emp}, V_{j+1}^{\rm emp}\right) &= \frac{2}{N^2}\sum_{p,q=1}^{3}\sum_{x,y\in\mathcal{G}_N} {\rm Cov}\left([\mathcal{M}X(\tau_x u_j)]_p, [\mathcal{M}X(\tau_y u_{j+1})]_q\right)^2 \\ &= \frac{2}{N^2}\sum_{p,q=1}^{3}\sum_{x,y\in\mathcal{G}_N} \mathcal{C}_{\mathcal{M}X}^{(p,q)}(\tau_x u_j, \tau_y u_{j+1})^2 \\ &= \frac{2}{N^2}\sum_{p,q=1}^{3}\sum_{x,y\in\mathcal{G}_N} \left|\int_{\mathbb{T}^2} e^{-i(x-y)\cdot\xi}\overline{g}_j^{(p,q)}(\xi)d\xi\right|^2, \end{aligned}$$

where instead of (41) we have now

$$\overline{g}_j^{(p,q)}(\xi) = \sum_{k\in\mathbb{Z}^2} C_{\mathcal{M}}^{(p,q)}(\xi+2k\pi)\widehat{u}_j(\xi+2k\pi)\overline{\widehat{u}_{j+1}(\xi+2k\pi)} f_{H,\delta}(\xi+2k\pi).$$

Then,

$$N^2 {\rm Cov}\left(V_j^{\rm emp}, V_{j+1}^{\rm emp}\right) = 2\sum_{p,q=1}^{3}\sum_{x\in\widetilde{\mathcal{G}}_N}\left(1-\frac{|x_1|}{N}\right)\left(1-\frac{|x_2|}{N}\right)\left|\int_{\mathbb{T}^2} e^{-ix\cdot\xi}\overline{g}_j^{(p,q)}(\xi)d\xi\right|^2$$

setting $\widetilde{\mathcal{G}}_N = \{-N+1,\dots,N-1\}^2$. In addition, by Parseval's identity,

$$\sum_{x\in\mathbb{Z}^2}\left|\int_{\mathbb{T}^2} e^{-ix\cdot\xi}\overline{g}_j^{(p,q)}(\xi)d\xi\right|^2 = (2\pi)^2\int_{\mathbb{T}^2}|\overline{g}_j^{(p,q)}(\xi)|^2 d\xi < +\infty,$$

since

$$\begin{aligned} \int_{\mathbb{T}^2}\left|\widehat{u}_j(\xi)\widehat{u}_{j+1}(\xi)\right|^2 f_{H,\delta}(\xi)^2 d\xi &\le \frac{1}{2}\left(\int_{\mathbb{T}^2}\left|\widehat{u}_j(\xi)\right|^4 f_{H,\delta}(\xi)^2 d\xi + \int_{\mathbb{T}^2}\left|\widehat{u}_{j+1}(\xi)\right|^4 f_{H,\delta}(\xi)^2 d\xi\right) \\ &< +\infty. \end{aligned}$$

It follows that the limit $\rho(u_j)$ exists and satisfies

$$\rho(u_j) = 8\pi^2\sum_{p,q=1}^{3}\int_{\mathbb{T}^2}|\overline{g}_j^{(p,q)}(\xi)|^2 d\xi.$$

Let us now set

$$\Sigma_j = \begin{pmatrix} \sigma^2(u_j) & \rho(u_j) \\ \rho(u_j) & \sigma^2(u_{j+1}) \end{pmatrix}$$

and write $H_j^{\rm emp} = F\left(V_j^{\rm emp}, V_{j+1}^{\rm emp}\right)$ with

$$F(x,y) = \frac{1}{2\log(2)}\log\left(\frac{x}{y}\right) - 1,\ x>0,\ y>0.$$

Since F is differentiable at $\left(\mathbb{E}\left(A_X(u_j)^2\right), \mathbb{E}\left(A_X(u_{j+1})^2\right)\right) \in (0,+\infty)^2$, by the Delta method, we obtain that

$$N\left(H_j^{\rm emp} - H\right) \xrightarrow[N\to\infty]{d} \mathcal{N}\left(0, \gamma^2(u_j)\right),$$

with the variance

$$\gamma^2(u_j) = \nabla F\left(\mathbb{E}\left(A_X(u_j)^2\right), \mathbb{E}\left(A_X(u_{j+1})^2\right)\right)^* \Sigma_j \nabla F\left(\mathbb{E}\left(A_X\left(u_j\right)^2\right), \mathbb{E}\left(A_X\left(u_{j+1}\right)^2\right)\right).$$

Then computing ∇F and recalling (22), one easily obtains (24).

Let us now assume that $\widehat{u}_j$ has support in $\mathbb{T}^2$. Then by the previous lines, and since $\sum_{p,q=1}^{3}|C_{\mathcal{M}}^{(p,q)}(\xi)|^2 = 4$,

$$\rho(u_j) = 32\pi^2\int_{\mathbb{T}^2}\left|\widehat{u}_j(\xi)\widehat{u}_{j+1}(\xi)\right|^2 f_{H,\delta}(\xi)^2 d\xi = 32\pi^2\int_{\mathbb{R}^2}\left|\widehat{u}_j(\xi)\widehat{u}_{j+1}(\xi)\right|^2 f_{H,\delta}(\xi)^2 d\xi$$

In addition, since $\widehat{u}_{j+1}(\xi) = 2\widehat{u}_j(2\xi)$, $\widehat{u}_{j+1}$ has also support in $\mathbb{T}^2$ and then by Corollary 5.3, we have

$$\begin{cases} \sigma^2(u_j) &= 32\pi^2\displaystyle\int_{\mathbb{R}^2}\left|\widehat{u}_j(\xi)\right|^4 f_{H,\delta}(\xi)^2 d\xi \\ \sigma^2(u_{j+1}) &= 32\pi^2\displaystyle\int_{\mathbb{R}^2}\left|\widehat{u}_{j+1}(\xi)\right|^4 f_{H,\delta}(\xi)^2 d\xi. \end{cases}$$

Therefore,

$$2^{4H+4}\sigma^2(u_j) - 2^{2H+3}\rho(u_j) + \sigma^2(u_{j+1}) = 32\pi^2 \int_{\mathbb{R}^2} \left(|\widehat{u}_{j+1}(\xi)|^2 - 2^{2H+2}\,|\widehat{u}_j(\xi)|^2\right)^2 f_{H,\delta}(\xi)^2 d\xi.$$

Moreover, we recall that by Theorem 3.7,

$$\mathbb{E}\left(A_X(u_{j+1})^2\right) = 2c_X(u_{j+1})$$

Hence, by (24),

$$\gamma^2(u_j) = \frac{2\pi^2}{(\log(2)c_X(u_{j+1}))^2} \int_{\mathbb{R}^2} \left(|\widehat{u}_{j+1}(\xi)|^2 - 2^{2H+2}\,|\widehat{u}_j(\xi)|^2\right)^2 f_{H,\delta}(\xi)^2 d\xi.$$

□

Proof of Proposition 6.2. It is enough to remark that

$$J_j^{\text{emp}} = \left[\mathcal{T}M_j^{\text{emp}}\right]_{2\le p,q\le 3},$$

Hence identifying this symmetric matrix with the $\mathbb{R}^3$ vector

$$([J_j^{\text{emp}}]^{(1,1)}, [J_j^{\text{emp}}]^{(2,2)}, [J_j^{\text{emp}}]^{(1,2)}) = (\mathcal{T}M_j^{\text{emp}}(2), \mathcal{T}M_j^{\text{emp}}(3), \mathcal{T}M_j^{\text{emp}}(6)),$$

using our previous vectorial identification. The asymptotic covariance matrix is given by $\Gamma_{\mathcal{R}}(u_j)$ where for $1 \le l, l' \le 3$

$$[\Gamma_{\mathcal{R}}(u_j)]_{l,l'} = [\Gamma_{\mathcal{T}M}(u_j)]_{p(l),p(l')},$$

with $p(1) = 2$, $p(2) = 3$ and $p(3) = 6$. Moreover, $\Gamma_{\mathcal{R}}(u_j) \neq 0$ since $[\Gamma_{\mathcal{T}M}(u_j)]_{p,p} \neq 0$ for $p \in \{2, 3\}$. □

Proof of Proposition 6.4. Let us introduce $F^{\pm} : \mathbb{R}^3 \to \mathbb{R}$ with

$$F^{\pm}(y_1, y_2, y_3) = \frac{1}{2}\left(y_1 + y_2 \pm \sqrt{(y_1 - y_2)^2 + 4y_3^2}\right),$$

for $(y_1, y_2, y_3) \in \mathbb{R}^3$ and remark that

$$\lambda_j^{\pm\text{emp}} = F^{\pm}\left(J_j^{\text{emp}}\right).$$

Since $F^{\pm}$ is differentiable at $J_X(u_j) := \left(\lambda^+(u_j), \lambda^-(u_j), 0\right)$ (still identifying the symmetric matrix with the $\mathbb{R}^3$ vector), the almost sure convergence follows from Proposition 6.2 and by continuity. In addition, the Delta method ensures the asymptotic normality (see Theorem 3.1 in [47] for instance). Moreover using the fact that $\nabla F^+\left(J_X(u_j)\right) = (1, 0, 0)$ and $\nabla F^-\left(J_X(u_j)\right) = (0, 1, 0)$, we obtain that

$$N\left(\begin{pmatrix} \lambda_j^{+\text{emp}} \\ \lambda_j^{-\text{emp}} \end{pmatrix} - \begin{pmatrix} \lambda_j^{+}(u_j) \\ \lambda_j^{-}(u_j) \end{pmatrix}\right) \xrightarrow[N\to+\infty]{d} \mathcal{N}(0, [\Gamma_{\mathcal{R}}\,(u_j)]_{1\le l,l'\le 2}) = \mathcal{N}(0, [\Gamma_{\mathcal{T}M}(u_j)]_{2\le l,l'\le 3}).$$

But recalling (43) the asymptotic covariance matrix satisfies, for $1 \le l, l' \le 2$,

$$[\Gamma_{\mathcal{R}}(u_j)]_{l,l'} = 8\pi^2 \int_{\mathbb{T}^2} |\overline{f}_j^{(l+1,l'+1)}(\xi)|^2 d\xi,$$

where $\overline{f}_j^{(l+1,l'+1)}$ is the periodisation of the function $C_{\mathcal{M}}^{(l+1,l'+1)}|\widehat{u}_j|^2 f_{H,\delta}$. It follows that when $\widehat{u}_j$ has support in $\mathbb{T}^2$ one has

$$\overline{f}_j^{(l+1,l'+1)}(\xi) = C_{\mathcal{M}}^{(l+1,l'+1)}(\xi)|\widehat{u}_j(\xi)|^2 f_{H,\delta}(\xi) = \frac{\xi_l \xi_{l'}}{|\xi|^2}|\widehat{u}_j(\xi)|^2 f_{H,\delta}(\xi),$$

that yields the result. □

Proof of Theorem 6.5. The strong consistency is an immediate consequence of Proposition 6.2. Moreover the asymptotic normality also follows from this proposition applying the Delta method for $F(x^+, x^-) = \frac{x^+ - x^-}{x^+ + x^-}$ which is differentiable in a neighborhood of $(\lambda^+(u_j), \lambda^-(u_j))$. Since

$$\nabla F(\lambda^+(u_j), \lambda^-(u_j)) = \frac{1}{c_X(u_j)}\left(1 + \frac{\sin(2\delta)}{2\delta}, -1 + \frac{\sin(2\delta)}{2\delta}\right),$$

$\sigma_\chi^2(u_j)c_X(u_j)^2$ is equal to

$$[\Gamma_{\mathcal{R}}(u_j)]_{1,1}\left(1 + \frac{\sin(2\delta)}{2\delta}\right)^2 + [\Gamma_{\mathcal{R}}(u_j)]_{2,2}\left(1 - \frac{\sin(2\delta)}{2\delta}\right)^2 - 2[\Gamma_{\mathcal{R}}(u_j)]_{1,2}\left(1 - \left(\frac{\sin(2\delta)}{2\delta}\right)^2\right).$$

Now assuming that $\widehat{u}_j$ has support in $\mathbb{T}^2$, by (A), one has

$$\sigma_\chi^2(u_j) = \frac{8\pi^2}{c_X(u_j)^2} \int_{\mathbb{R}^2} \left(\frac{\xi_1^2}{|\xi|^2} - \frac{\xi_2^2}{|\xi|^2} + \frac{\sin(2\delta)}{2\delta}\right)^2 |\widehat{u}_j(\xi)|^4 f_{H,\delta}(\xi)^2 d\xi.$$

Hence setting $\mathrm{e}_1 = (1, 0)$ and using a change of variables in polar coordinates one has

$$\sigma_\chi^2(u_j) = \frac{16\pi^2}{c_X(u_j)^2} \int_0^{+\infty} \int_{-\delta}^{\delta} \left(\cos(2\alpha) + \frac{\sin(2\delta)}{2\delta}\right)^2 |\widehat{u}_j(r\mathrm{e}_1)|^4\, r^{-2(2H+2)+1} d\alpha dr$$

since $\widehat{u}$ is a radial function. But

$$\begin{aligned}\int_{-\delta}^{\delta}\left(\cos(2\alpha)+\frac{\sin(2\delta)}{2\delta}\right)^2 d\alpha &= \delta+\frac{\sin(4\delta)}{4}+2\frac{\sin(2\delta)}{2\delta}\sin(2\delta)+2\delta\left(\frac{\sin(2\delta)}{2\delta}\right)^2\\ &= \delta+\frac{\sin(4\delta)}{4}+3\frac{\sin(2\delta)^2}{2\delta}.\end{aligned}$$

Therefore,

$$\sigma_\chi^2(u_j)=\frac{(2\pi)^2}{c_X(u_j)^2}\left(1+\frac{\sin(4\delta)}{4\delta}+\frac{3}{2}\left(\frac{\sin(2\delta)}{2\delta}\right)^2\right)\int_{\mathbb{R}^2}|\widehat{u}_j(\xi)|^4 f_{H,\delta}(\xi)^2 d\xi$$

which concludes the proof. □

References

[1] P. Abry and F. Sellan. The wavelet-based synthesis for fractional Brownian motion proposed by F. Sellan and Y. Meyer: remarks and fast implementation. *Appl. Comput. Harmon. Anal.*, 3:377–383, 1996.

[2] P. Abry and D. Veitch. Wavelet analysis of long-range-dependent traffic. *IEEE Transactions on Information Theory*, 44:2–15, 1998.

[3] D. Allard, R. Senoussi, and E. Porcu. Anisotropy models for spatial data. *Mathematical Geosciences*, 48, 2016.

[4] M. A. Arcones. Limit theorems for nonlinear functionals of a stationary Gaussian sequence of vectors. *The Annals of Probability*, 22(4):2242–2274, 1994.

[5] J.-M. Bardet. Statistical study of the wavelet analysis of fractional Brownian motion. *IEEE Trans. Inform. Theory*, 48(4):991–999, 2002.

[6] J.-M. Bardet, G. Lang, G. Oppenheim, A. Philippe, S. Stoev, and M. S. Taqqu. Semi-parametric estimation of the long-range dependence parameter: a survey. In *Theory and applications of long-range dependence*, pages 557–577. Birkhäuser Boston, Boston, MA, 2003.

[7] A. Benassi, S. Cohen, J. Istas, and S. Jaffard. Identification of filtered white noises. *Stochastic Process. Appl.*, 75(1):31–49, 1998.

[8] D. Benson, M. M. Meerschaert, B. Bäumer, and H. P. Scheffler. Aquifer operator-scaling and the effect on solute mixing and dispersion. *Water Resour. Res.*, 42:1–18, 2006.

[9] H. Biermé. Introduction to random fields and scale invariance. *Stochastic Geometry: Modern Research Frontiers*, pages 129–180, 2019.

[10] H. Biermé, C.L. Benhamou, and F. Richard. Parametric estimation for Gaussian operator scaling random fields and anisotropy analysis of bone radiograph textures. In K. Pohl, editor, *Proc. of the International Conference on Medical Image Computing and Computer Assisted Intervention (MICCAI'09), Workshop on Probabilistic Model s for Medical Imaging*, pages 13–24, London, UK, september 2009.

[11] H. Biermé, A. Bonami, and León J. R. Central limit theorems and quadratic variations in terms of spectral density. *Electronic Journal of Probability*, 16(3):362–395, 2011.

[12] H. Biermé, O. Durieu, and Y. Wang. Generalized random fields and Lévy's continuity theorem on the space of tempered distributions. *Commun. Stoch. Anal.*, 12(4):Art. 4, 427–445, 2018.

[13] H. Biermé, M. M. Meerschaert, and H. P. Scheffler. Operator scaling stable random fields. *Stoch. Proc. Appl.*, 117(3):312–332, 2007.

[14] H. Biermé, L. Moisan, and F. Richard. A turning-band method for the simulation of anisotropic fractional Brownian fields. *J. Comput. Graph. Statist*, 24(3), 2015.

[15] H. Biermé and F. Richard. Estimation of anisotropic Gaussian fields through Radon transform. *ESAIM Probab. Stat.*, 12:30–50, 2008.

[16] A. Bonami and A. Estrade. Anisotropic analysis of some Gaussian models. *The Journ. Fourier Analysis and Applic.*, 9:215–239, 2003.

[17] T. Candela, M. Bouchon, A. Brouste, D. Marsan, J. Schmittbuhl, and C. Voisin. Characterization of fault roughness at various scales: Implications of three-dimensional high resolution topography measurements. *Pure and Applied Geophysics*, 166((10-11)):1817–1851, 2009.

[18] G. Chan and A. T. A. Wood. Increment-based estimators of fractal dimension for two-dimensional surface data. *Statist. Sinica*, 10(2):343–376, 2000.

[19] J.-F. Coeurjolly. Estimating the parameters of a fractional Brownian motion by discrete variations of its sample paths. *Stat. Inference Stoch. Process.*, 4(2):199–227, 2001.

[20] J.F. Coeurjolly. Simulation and identification of the fractional Brownian motion: a bibliographical and comparative study. *Journal of Statistical Software*, 5:1–53, 2000.

[21] S. Davies and P. Hall. Fractal analysis of surface roughness by using spatial data. *J. R. Stat. Soc. Ser. B*, 61:3–37, 1999.

[22] L. Davy, N. Pustelnik, and P. Abry. Combining dual-tree wavelet analysis and proximal optimization for anisotropic scale-free texture segmentation. In *ICASSP 2023-2023 IEEE International Conference on Acoustics, Speech and Signal Processing (ICASSP)*, pages 1–5. IEEE, 2023.

[23] L. Delbeke and P. Abry. Stochastic integral representation and properties of the wavelet coefficients of linear fractional stable motion. *Stochastic Processes and their Applications*, 86(2):177–182, 2000.

[24] M. Felsberg and G. Sommer. The monogenic signal. *IEEE Trans. on Signal Proc.*, 49(12), 2001.
[25] C. Feng, Y. Mei, and B. Vidakovic. *Mammogram Diagnostics Using Robust Wavelet-Based Estimator of Hurst Exponent*, pages 109–140. Springer International Publishing, 01 2018.
[26] X. Guyon. *Random fields on a network*. Probability and its Applications (New York). Springer-Verlag, New York, 1995. Modeling, statistics, and applications, Translated from the 1992 French original by Carenne Ludeña.
[27] J. Istas and G. Lang. Quadratic variations and estimation of the local Hölder index of a Gaussian process. *Ann. Inst. H. Poincaré Probab. Statist.*, 33(4):407–436, 1997.
[28] S. Rao Jammalamadaka and A. SenGupta. *Topics in circular statistics*, volume 5 of *Series on Multivariate Analysis*. World Scientific Publishing Co., Inc., River Edge, NJ, 2001. With 1 IBM-PC floppy disk (3.5 inch; HD).
[29] A. Kamont. On the fractional anisotropic Wiener field. *Probab. Math. Statist.*, 16:85–98, 1996.
[30] M. Kang and B. Vidakovic. Medl and medla: Methods for assessment of scaling by medians of log-squared non-decimated wavelet coefficients. Technical report, arXiv, 2017.
[31] A. N. Kolmogorov. Wienersche Spiralen und einige andere interessante Kurven in Hilbertsche Raum. *C. R. (Dokl.) Acad. Sci. URSS*, 26:115–118, 1940.
[32] S. Léger and M. Pontier. Drap brownien fractionnaire. *Comptes Rendus de l'Académie des Sciences-Series I-Mathematics*, 329(10):893–898, 1999.
[33] J. Lévy Véhel. *Fractals in engineering: from theory to industrial applications*. Springer, New York, 1997.
[34] R. Lopes and N. Betrouni. Fractal and multifractal analysis: a review. *Med Image Anal.*, 13(4):634–649, 2009.
[35] S. Mallat and S. Zhong. Characterization of signals from multiscale edges. *IEEE Transactions on Pattern Analysis & Machine Intelligence*, 14(07):710–732, 1992.
[36] B. B. Mandelbrot and J. Van Ness. Fractional Brownian motion, fractional noises and applications. *SIAM Review*, 10:422–437, 1968.
[37] S. C. Olhede, D. Ramírez, and P. J. Schreier. Detecting directionality in random fields using the monogenic signal. *IEEE Trans. Inform. Theory*, 60(10):6491–6510, 2014.
[38] G. Peccati and C. A. Tudor. Gaussian limits for vector-valued multiple stochastic integrals. *Séminaire de Probabilités XXXVIII*, pages 247–262, 2005.
[39] V. Pipiras and M. S. Taqqu. Regularization and integral representations of Hermite processes. *Statist. Probab. Lett.*, 80(23-24):2014–2023, 2010.
[40] K. Polisano. *Modélisation de textures anisotropes par la transformée en ondelettes monogéniques*. PhD thesis, Université Grenoble Alpes, December 2017.
[41] K. Polisano, M. Clausel, V. Perrier, and L. Condat. Riesz-based orientation of localizable Gaussian fields. *Appl. Comput. Harmon. Anal.*, 50:353–385, 2021.
[42] F. J.P. Richard. PyAFBF: a Python library for sampling image textures from the anisotropic fractional Brownian field. *Journal of Open Source Software*, 7(75):3821, 2022.
[43] G. Samorodnitsky and M. S. Taqqu. *Stable non-Gaussian random processes*. Stochastic Modeling. Chapman & Hall, New York, 1994. Stochastic models with infinite variance.
[44] S. Soltani, P. Simard, and D. Boichu. Estimation of the self-similarity parameter using the wavelet transform. *Signal Processing*, 84(1):117–123, 2004.
[45] R. Soulard and P. Carré. Characterization of color images with multiscale monogenic maxima. *IEEE Trans on Pattern Analysis and Machine Intel.*, 40(10), 2018.
[46] E. M. Stein. *Harmonic analysis: real-variable methods, orthogonality, and oscillatory integrals*, volume 43 of *Princeton Mathematical Series*. Princeton University Press, Princeton, NJ, 1993. With the assistance of Timothy S. Murphy, Monographs in Harmonic Analysis, III.
[47] A. W. van der Vaart. *Asymptotic statistics*, volume 3 of *Cambridge Series in Statistical and Probabilistic Mathematics*. Cambridge University Press, Cambridge, 1998.
[48] D. Veitch and P. Abry. A wavelet-based joint estimator of the parameters of long-range dependence. *IEEE Transactions on Information Theory*, 45:878–897, 1999.
[49] W. Willinger, V. Paxson, and M. S. Taqqu. Self-similarity and heavy tails: Structural modeling of network traffic. In *A practical guide to heavy tails (Santa Barbara, CA, 1995)*, pages 27–53. Birkhäuser Boston, Boston, MA, 1998.

Hermine Biermé, IDP, Université de Tours, Parc Grandmont, 37200 Tours, France.
Email address: hermine.bierme@univ-tours.fr

Philippe Carré, Université de Poitiers, Téléport 2-BP30179, Boulevard Marie et Pierre Curie, 86962 Chasseneuil, France.
Email address: philippe.carre@univ-poitiers.fr

Céline Lacaux, Laboratoire de Mathématiques d'Avignon, UPR 2151, Avignon Université, 84000 Avignon, France.
Email address: Celine.Lacaux@univ-avignon.fr

Claire Launay, Université Bretagne Sud, UMR CNRS 6205, LMBA, F-56000 Vannes, France
Email address: claire.launay@univ-ubs.fr